

## CHAPTER 4

DEBUNCHER RING4.1 Purpose of the Debuncher

The primary purpose of the Debuncher is to reduce the large momentum spread of the 8-GeV  $\bar{p}$  beam at production to 0.2% or less prior to injection into the Accumulator. This reduction is done by rf bunch rotation and adiabatic debunching after the  $\bar{p}$  beam is injected into stationary 53-MHz buckets in the Debuncher. The debunching time is only slightly longer than 10 msec, and there are therefore nearly two seconds available for cooling before the beam is transferred to the Accumulator. Stochastic cooling of betatron amplitudes has been shown to be feasible, and a betatron cooling system to reduce the emittance by a factor of 3 in both planes in 2 sec is included in the design.

A possible addition that is still being examined is a fast momentum stochastic precooling step to reduce even further the momentum spread by a factor of 2 or possibly 3, in 2 sec.

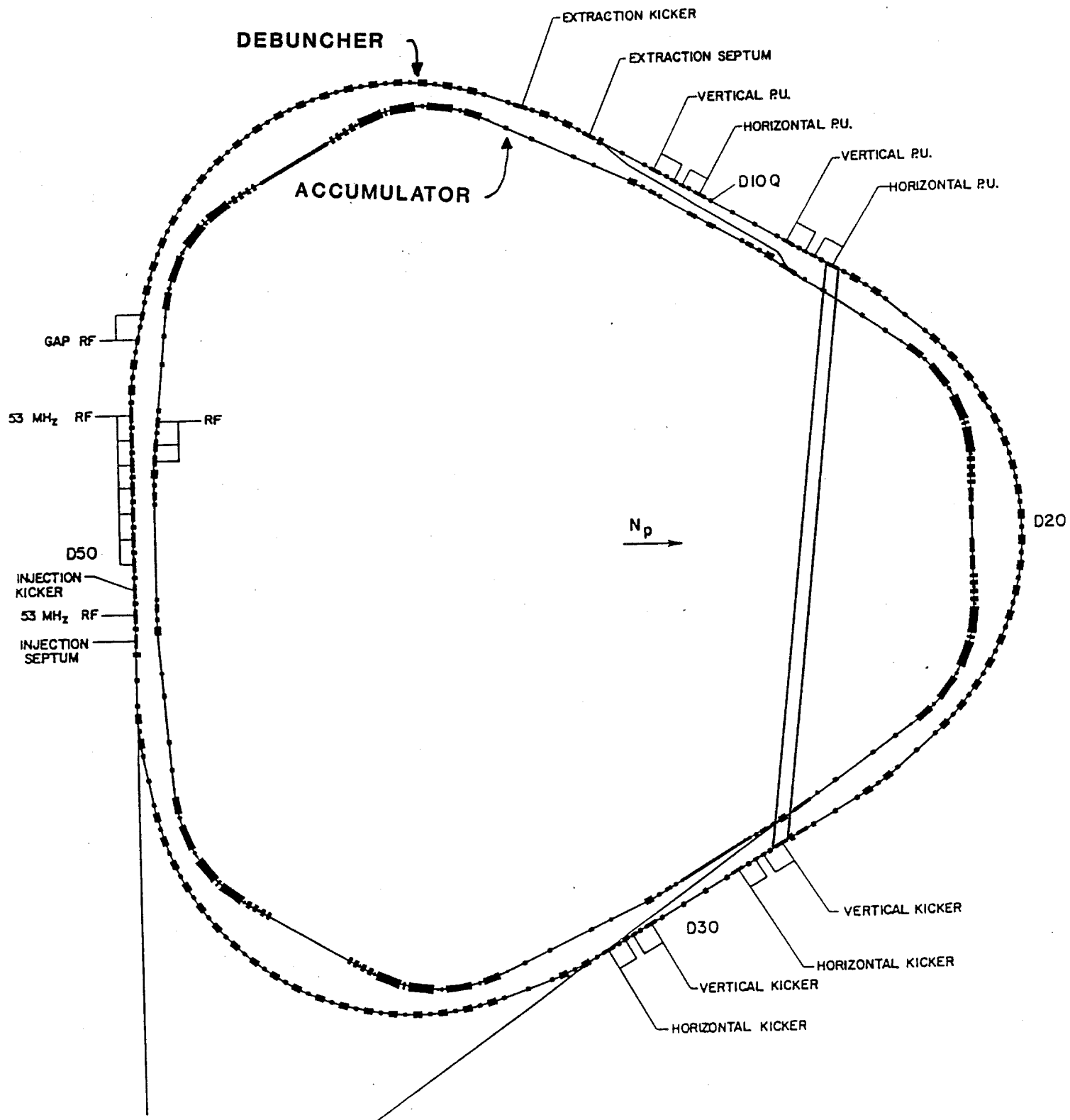
Table 4-I gives parameters of the Debuncher.

TABLE 4-I THE DEBUNCHER RING

|                                      |                              |
|--------------------------------------|------------------------------|
| Kinetic Energy                       | 8.0 GeV                      |
| $\gamma_t$ , transition energy       | 7.6482                       |
| $\eta = 1/\gamma_t^2 - 1/\gamma^2$   | 0.00608                      |
| Average Radius                       | 80.42 m                      |
| RF Frequency                         | 53.103 MHz                   |
| Maximum rf voltage                   | 5 MV                         |
| Number of $\bar{p}$ bunches injected | 80                           |
| Harmonic number                      | 90                           |
| Beam Gap for Injection Kicker        | 200 nsec                     |
| Momentum Aperture, $\Delta p/p$      | 4%                           |
| Betatron Acceptance, h and v         | $20\pi$ mm-mrad              |
| Betatron Tunes, h and v              | 9.75                         |
| Natural Chromaticity, h and v        | -10                          |
| Periodicity                          | 3, each with mirror symmetry |
| Max amplitude function $\beta$       | 20 m                         |
| Max dispersion value                 | 2.1 m                        |
| Phase Advance per Cell, h and v      | $60^\circ$                   |

4.2 Requirements of the Design

As shown in Fig. 4-1, the Debuncher ring surrounds the Accumulator. Because of the triangular shape of the latter, a periodicity of three was chosen for the Debuncher, each period with mirror symmetry.



**DEBUNCHER LAYOUT**

Figure 4-1

The Debuncher operates at a kinetic energy of 8 GeV. Its circumference must be at least as long as each antiproton pulse, made of 80 narrow bunches with a separation frequency of 53.1 MHz. The circumference was chosen to be 505 m, which corresponds to an rf harmonic number of 90. This arrangement allows a separation of 12 ft between the Debuncher and the Accumulator in the long straight sections so that these portions of the two rings can be accommodated in the same wide tunnel.

Each superperiod includes a long straight section. These accommodate: (i) injection, (ii) extraction, (iii) rf cavities for the bunch rotation, (iv) pickups and kickers for stochastic cooling. The phase advance between pickups and kickers should be an integer number of betatron waves  $\pm 90^\circ$ . This gives only a few possible choices for betatron tunes, which we take to be approximately the same in the two planes. The value 9.75 was finally chosen.

Another requirement is that the three long straight sections must have zero dispersion, an important requirement for the performance of stochastic cooling and for avoiding betatron-synchrotron coupling.

Finally the Debuncher is capable of accepting a momentum spread of  $\pm 2\%$  and has a betatron acceptance of at least  $20\pi$  mm-mrad in both planes.

#### 4.3 Choice of Transition Energy

The most important parameter in the design of the Debuncher is the dispersion

$$\eta = 1/\gamma_t^2 - 1/\gamma^2$$

where  $\gamma$  is the relativistic energy factor and  $\gamma_t$  corresponds to the transition energy. The rf voltage needed for bunch rotation is proportional to  $|\eta|$ . If  $|\eta|$  is less than 0.002, the variation of  $\eta$  with momentum will degrade the final momentum spread. On the other hand, a larger value of  $|\eta|$  helps betatron cooling and is needed if momentum precooling is to be done in the future. We have reached a compromise by setting  $\eta=0.006$ , which corresponds to  $\gamma_t=7.65$ , a solution which gives  $v_H/v$  approximately 9.75. This choice corresponds to operating the Debuncher Ring above the transition energy.

We could also have chosen to operate below the transition energy (larger value of  $\gamma_t$ ) because only the absolute value of  $\eta$  enters. We considered this possibility at the beginning of the design, but rejected it for the following reasons. A larger value of  $\gamma_t$ , and therefore of the strength of the lattice focusing, is desirable because it makes the dispersion and betatron amplitude functions small, which would also make the physical aperture of the magnets smaller. But larger values of  $\gamma_t$  would also lead to an unfortunately large natural chromaticity. To correct this, too much sextupole correction was required considering the smaller

dispersion around the ring. To eliminate problems intrinsic to sextupoles and chromaticity, we had to decrease the focusing of the ring to the present value of  $\gamma_t=7.65$ . When this was done, the dispersion of the ring doubled, but we could still manage to achieve the required momentum and betatron acceptance with reasonably small-aperture magnets.

With this choice of  $\eta$ , one still requires 5 MV peak rf voltage at 53 MHz for bunch rotation.

#### 4.4 Lattice

We have opted for a smooth lattice to help stability of the ring against sextupoles and chromatic effects. The ring is divided into 57 FODO cells, each with a phase advance of  $60^\circ$  in each plane. One half a superperiod is shown in Fig. 4-2 with beta- and dispersion-function plots. In the curved sections of the ring, the cells are regular; bending magnets are placed exactly halfway between quads. The long straight sections are made of 6 cells, each without bending magnets. A "dispersion-killer" cell is located at each end of the long straight section. Zero dispersion is achieved by eliminating the two bending magnets just before the last regular cell. A regular cell is shown in Fig. 4-3.

Two fortunate features are obtained with this lattice: (i) the beta functions never exceed 20 m in either plane. This makes the beam size in the long straight sections small enough to fit in the aperture of stochastic-cooling pickups and kickers, which have a gap between plates of 30 mm (suitable for 2-4 GHz bandwidth). (ii) The chromaticity of the ring is reduced to a minimum of -10. In an earlier design, each long straight section was made of three consecutive low-beta insertions. To do this, four quadrupole triplets were required to provide room for stochastic-cooling devices, rf cavities and injection and extraction equipment. It has been found that these triplets added substantially to the natural chromaticity and it was therefore decided to bridge the long straight sections with regular FODO cells.

The beam envelope is shown in Fig. 4-4 for half of a superperiod. It corresponds to a momentum spread of 3% and an emittance of  $20\pi$  mm-mrad in both planes.

#### 4.5 Magnets

There is only one kind of dipole in the design. The dipoles are 1.66 m long (effective length), have a full gap of 6 cm and have a strength of 17 kG. There are three kinds of quadrupoles. The dipole and quadrupoles are described in Table 4-II. There is one kind of sextupole. The sextupoles are discussed in Sec. 4.7.

# Debuncher Lattice Functions For One Sextant

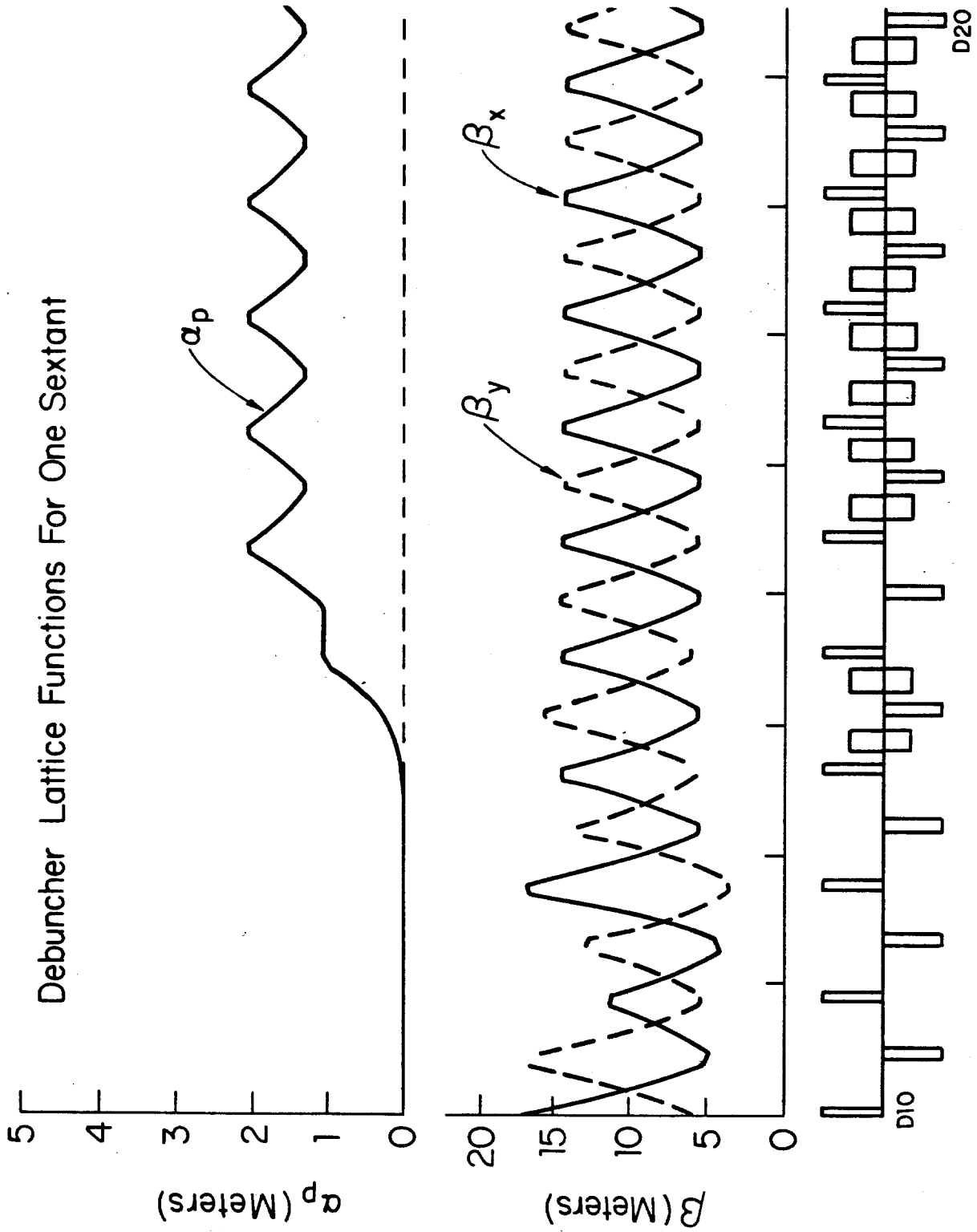


Figure 4-2

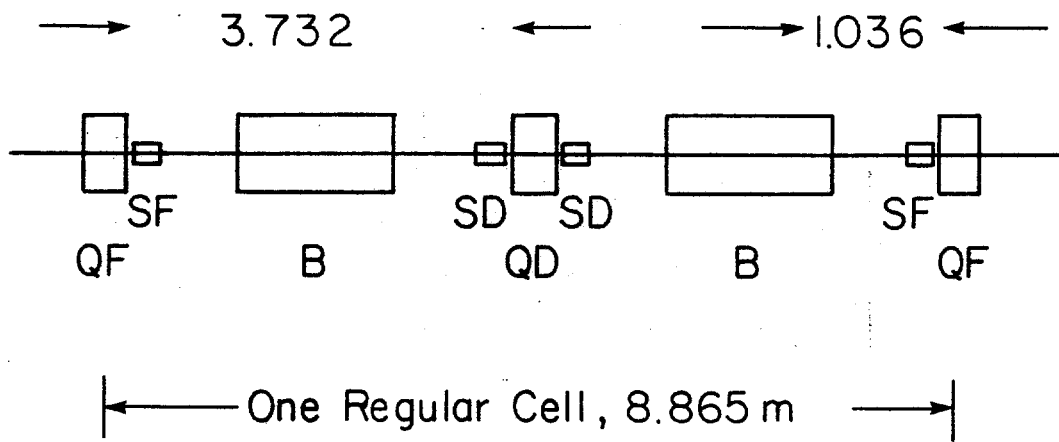
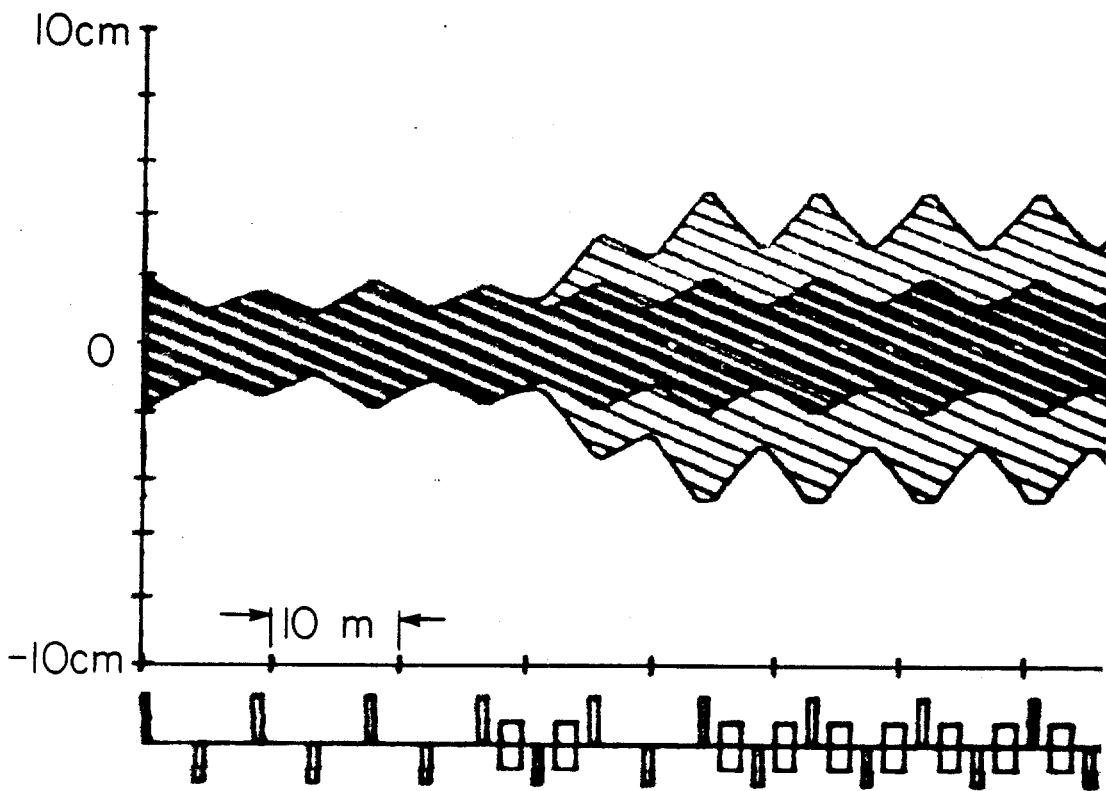


Figure 4-3



**Horizontal Beam Envelopes for  
 $\Delta P/P = 3\%$  and  $E = 20\pi$  mm-mrad  
 Before and After Debunching**



TABLE 4-II DEBUNCHER MAGNETS

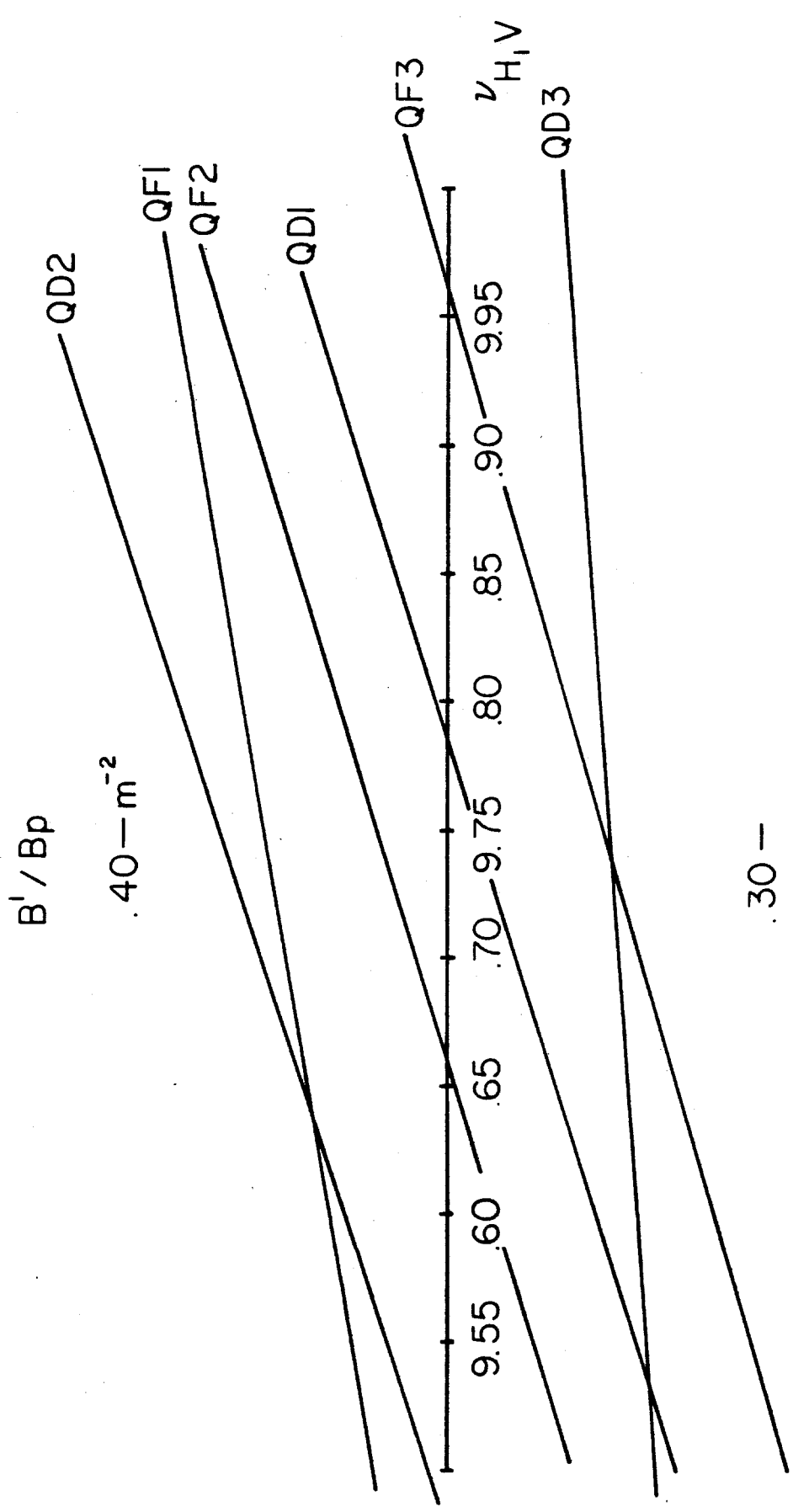
|                                   | <u>Number</u> | <u>Effective Length</u> | <u>Strength</u> | <u>Gap or Poletip Radius</u> |
|-----------------------------------|---------------|-------------------------|-----------------|------------------------------|
| Dipoles:                          |               |                         |                 |                              |
| B                                 | 66            | 1.6604 m                | 1.7 T           | 66 mm                        |
| Quadrupoles:                      |               |                         |                 |                              |
| I. QF, QD<br>QF1, QD1<br>QF2, QD2 | 102           | 27.6 in.                | 12 T/m          | 44.5 mm                      |
| II. QF3, QD3<br>small aperture    | 9             | 32.6 in.                | 10.5 T/m        | 44.5 mm                      |
| III. QF3, QD3<br>large aperture   | 3             | 32.6 in.                | 10.5 T/m        | 84.1 mm                      |

There are two effective quadrupole lengths: 27.6 in. and 32.6 in. The longer quadrupoles are located in pairs at both ends of each long straight section as shown in Fig. 4-5 which shows a long straight section with the neighboring regular cells. All the other quadrupoles are shorter. All quadrupoles have the same aperture, with a poletip radius of 44.5 mm, except for three special ones that have a poletip radius of 84.1 mm. These quadrupoles are marked with an L in Fig. 4-1 and are also used in conjunction with beam transfer from and to several directions. The maximum gradient required is 12 T/m and somewhat less for the large aperture quadrupoles. The total magnet power to operate the ring at 8 GeV is 1.1 MW.

A detailed set of specifications for the magnets is given in Chapter 12.

#### 4.6 Tuning

A nominal tuning mode has been worked out with betatron numbers  $\nu_H=9.73$  and  $\nu_V=9.77$ . To obtain this, the regular cells have exactly  $60^\circ$  phase advance in both planes to give zero dispersion in the long straight sections. The quadrupoles in the long straight sections have been adjusted to get the required tune values with proper matching at the transition between the curved and straight sections. A waist is introduced in the middle of each long straight section and curved sector. The settings for all the magnets are given in Table 4-III for the nominal tune.



.30 -

Variation Of  $B'/B$  For Each Type Of Quadrupole

Figure 4-6

TABLE 4-III MAGNET SETTING FOR THE TUNING MODE:  $\nu_H=9.73$ ,  $\nu_v=9.77$ 

B = 1.7 T  
 $B\rho = 29.6501$  T-m

| <u>Quadrupoles</u> | <u><math>B_q/B\rho</math></u> | <u>Current</u> | <u>Voltage</u> |
|--------------------|-------------------------------|----------------|----------------|
| QF                 | 0.33652 $m^{-2}$              | 240 A          | 9.7 V          |
| QD                 | 0.32928                       | 235            | 9.5            |
| QF1                | 0.37747                       | 270            | 10.9           |
| QD1                | 0.34714                       | 248            | 10.0           |
| QF2                | 0.35881                       | 256            | 10.3           |
| QD2                | 0.38679                       | 276            | 11.1           |
| QF3 large          | 0.32494                       | 1313           | 10.5           |
| QD3 aperture       | 0.32459                       | 1311           | 10.5           |
| QF3 small          | 0.32494                       | 232            | 10.4           |
| QD3 aperture       | 0.32459                       | 232            | 10.4           |

To achieve other betatron tune values, the strength of the regular quadrupoles QF and QD in the bending section is left unchanged, so that the phase advance/cell will remain  $60^\circ$ . With this mode of operation, the "dispersion killer" is always effective and the dispersion in the long straight section is always cancelled. To change the betatron tune, only the strengths of the six quadrupoles QF1, QD1, QF2, QD2, QF3 and QD3 in the long straight sections are varied. The search for the quadrupole setting is done by imposing the condition of matching between the long straight sections and the curved sections and of waists in the middle of both of them. It is possible to vary both tunes over the range from 9.5 to 10.0 by keeping them equal. The variation of  $B_q/B\rho$  for each quad is shown in Fig. 4-6. The transition energy remains unchanged in this range. The variation of  $\beta_H$  and  $\beta_V$ , the maximum values of the horizontal and vertical beta functions in the space occupied by the pickups and kickers for the stochastic cooling, is given in Fig. 4-7. In the same figure, we give the variations of the natural horizontal and vertical chromaticities.

#### 4.7 Sextupoles

Sextupoles are located next to each quadrupole, usually on both sides, as shown in Fig. 4-2. They are divided in two groups: those next to the horizontally focusing quads (SF) and those next to the vertically focusing quads (SD). The main purpose of these sextupoles is to correct and adjust the natural chromaticity of the ring. They are therefore elements of primary importance and are on an equal footing with the dipoles and quadrupoles. They are not intended to correct magnet errors and imperfections.

Their strength has been calculated with PATRIS, a particle tracking code that is a heavily modified version of PATRICIA suitable for protons.

# Variation Of Lattice Functions Across A Cooling Straight Section

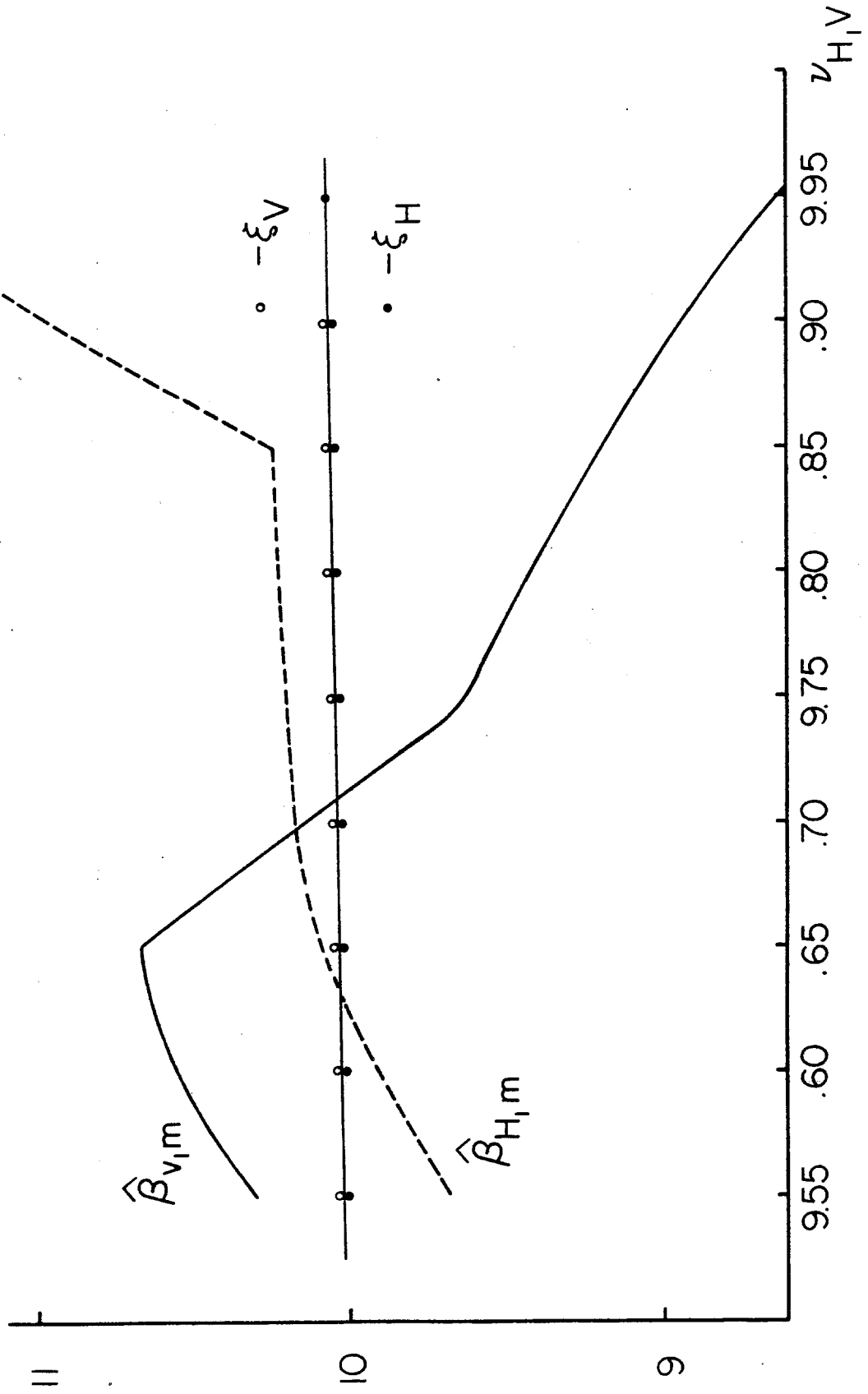
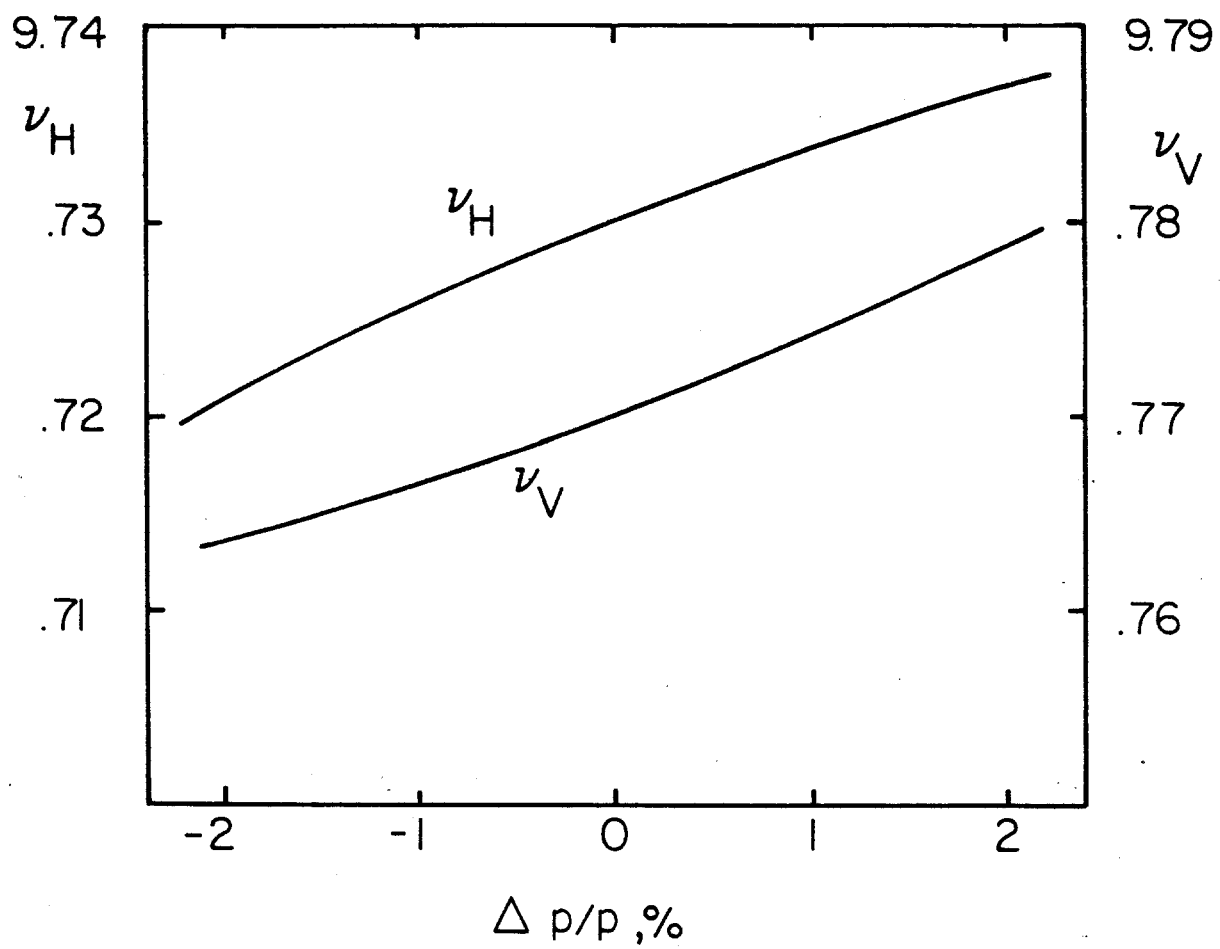


Figure 4-7



**Variation Of Tunes With Momentum**

Figure 4-8

The thin-lens approximation has been used. The sextupole strength given in Table 4-IV corresponds to zero chromaticity. The lattice variations with momentum have then been calculated with SYNCH. The results are shown in Fig. 4-8, which gives the variation of the betatron tunes with momentum, Fig. 4-9, which gives the change of  $\alpha = 1/\gamma_t^2$ , the momentum compaction factor, and Fig. 4-10 which gives  $\beta_H$ ,  $\beta_V$  and  $\alpha_D$  versus  $\Delta p/p$  at the downstream end of the injection kicker. Figure 4-11 gives the tune diagram with the working point for the reference tuning mode and the tune spread for  $\pm 2\%$  beam momentum spread. Finally, Fig. 4-12 gives the variation of  $\beta$  with momentum along the ring circumference for half of a superperiod. As one can see, the variations are very modest, less than 10%.

TABLE 4-IV DEBUNCHER SEXTUPOLE DISTRIBUTION

| Type            | SF                     | SD                      |
|-----------------|------------------------|-------------------------|
| Number          | 72                     | 66                      |
| $B''\ell/B\rho$ | $0.141 \text{ m}^{-2}$ | $-0.213 \text{ m}^{-2}$ |

The design specifications for the sextupoles are given in Table 4-V. The power per magnet is so small that no water cooling is needed.

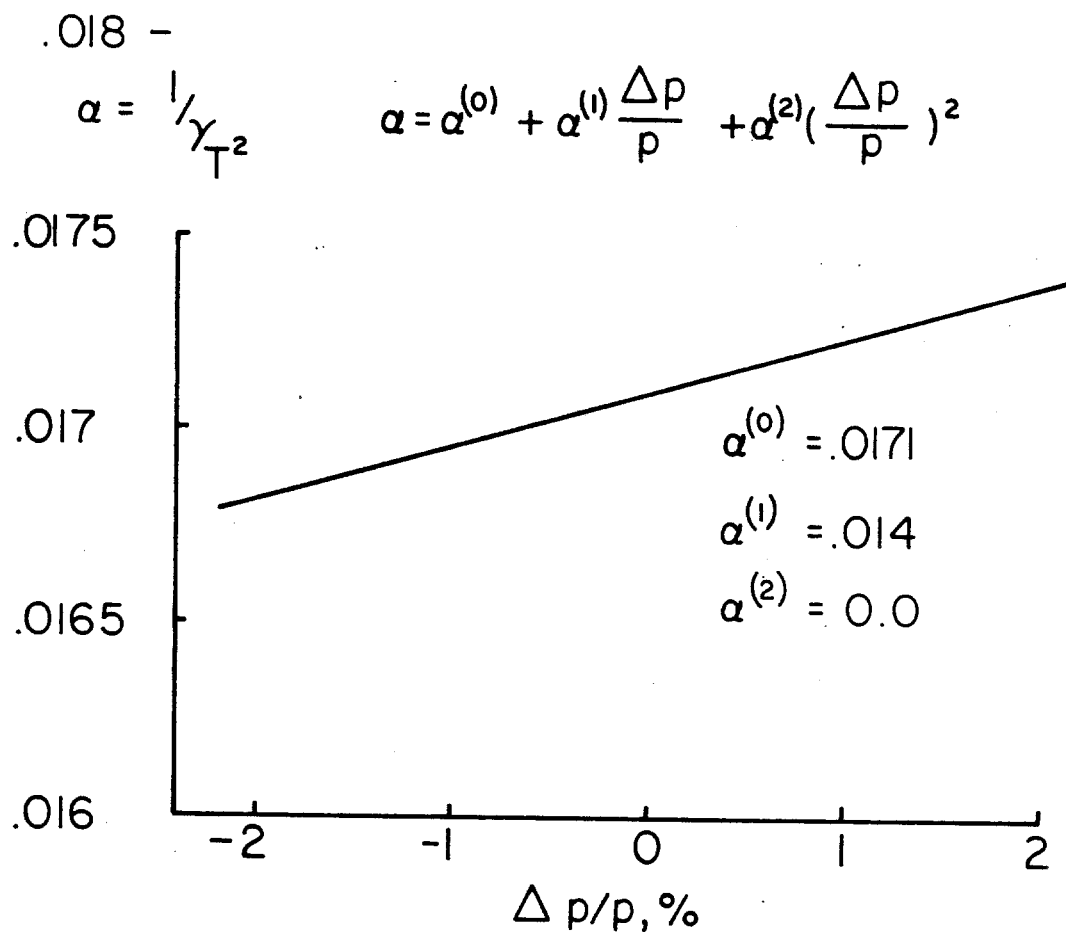
TABLE 4-V DEBUNCHER SEXTUPOLE MAGNETS

|                                   |                                                               |
|-----------------------------------|---------------------------------------------------------------|
| Maximum strength, $B''\ell/B\rho$ | $0.22 \text{ m}^{-2}$                                         |
| Bore radius                       | 70 mm                                                         |
| Effective length                  | 0.2 m                                                         |
| Maximum field, $B''$              | $33 \text{ T/m}^2$                                            |
| Ampere-turns                      | 1555 AT/pole                                                  |
| Current                           | 256 A                                                         |
| Turns                             | 6 turns/pole                                                  |
| Conductor size                    | 0.3294" square, 0.18" hole dia., area $0.07723 \text{ in.}^2$ |
| Current density                   | $3.35 \text{ kA/in.}^2$                                       |
| Resistance                        | $5 \text{ m}\Omega/\text{magnet}$                             |
| Voltage Drop                      | $1.45 \text{ V/magnet}$                                       |
| Thermal loss                      | $375 \text{ W/magnet}$                                        |

#### 4.8 Magnet Power Supplies

The layouts of the magnet power supplies and their circuits are dictated by the operating mode of the Debuncher Ring. The situation can be summarized as follows

- i) There will be one individually controlled power supply bus for each family of sextupoles, SF and SD. The current is 80 A and 120 A respectively with a regulation of 0.1%. A tunability range of  $\pm 10\%$  is desirable for chromaticity control over a wider range.



**Variation Of Momentum-Compaction Factor With Momentum**

# Variation Of Lattice Functions With Momentum At The Injection Kicker

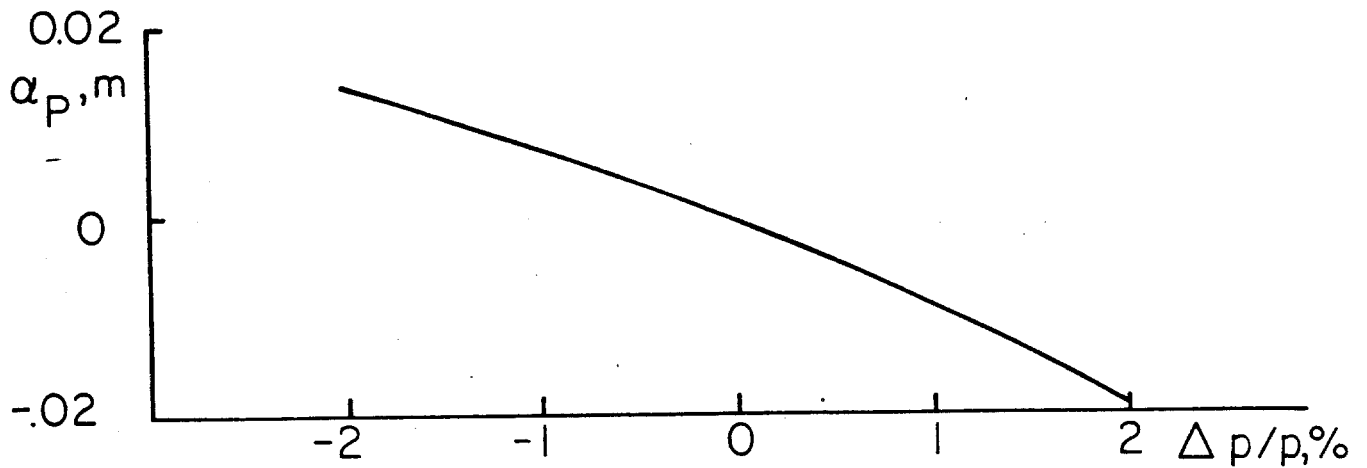
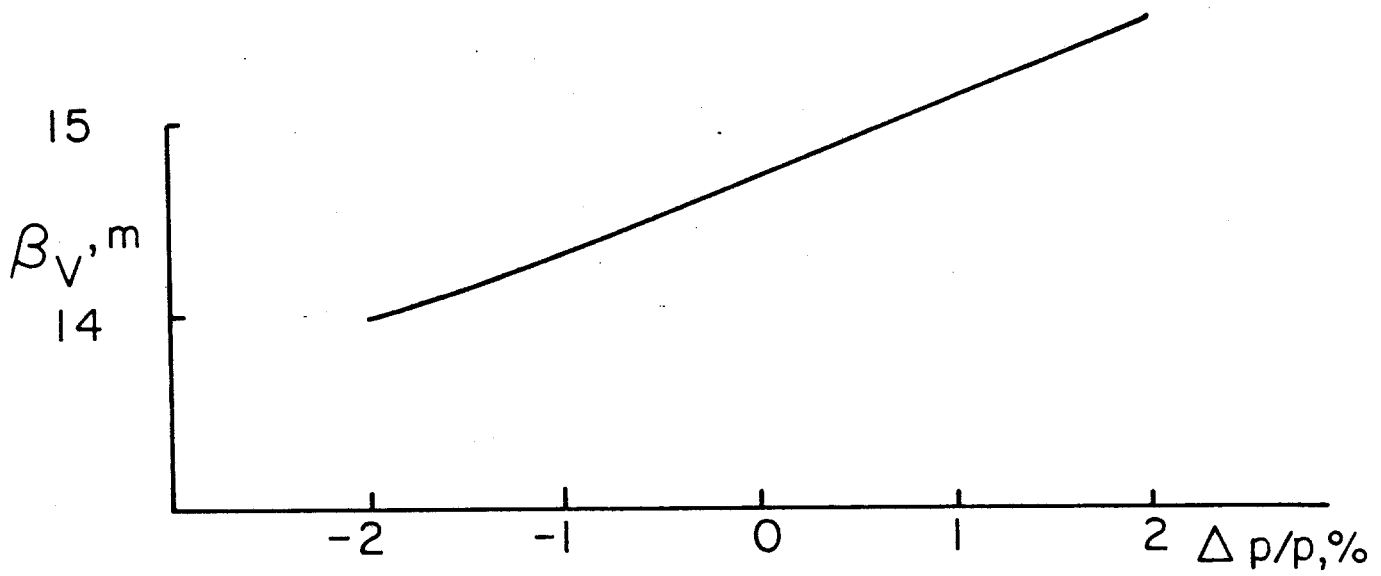
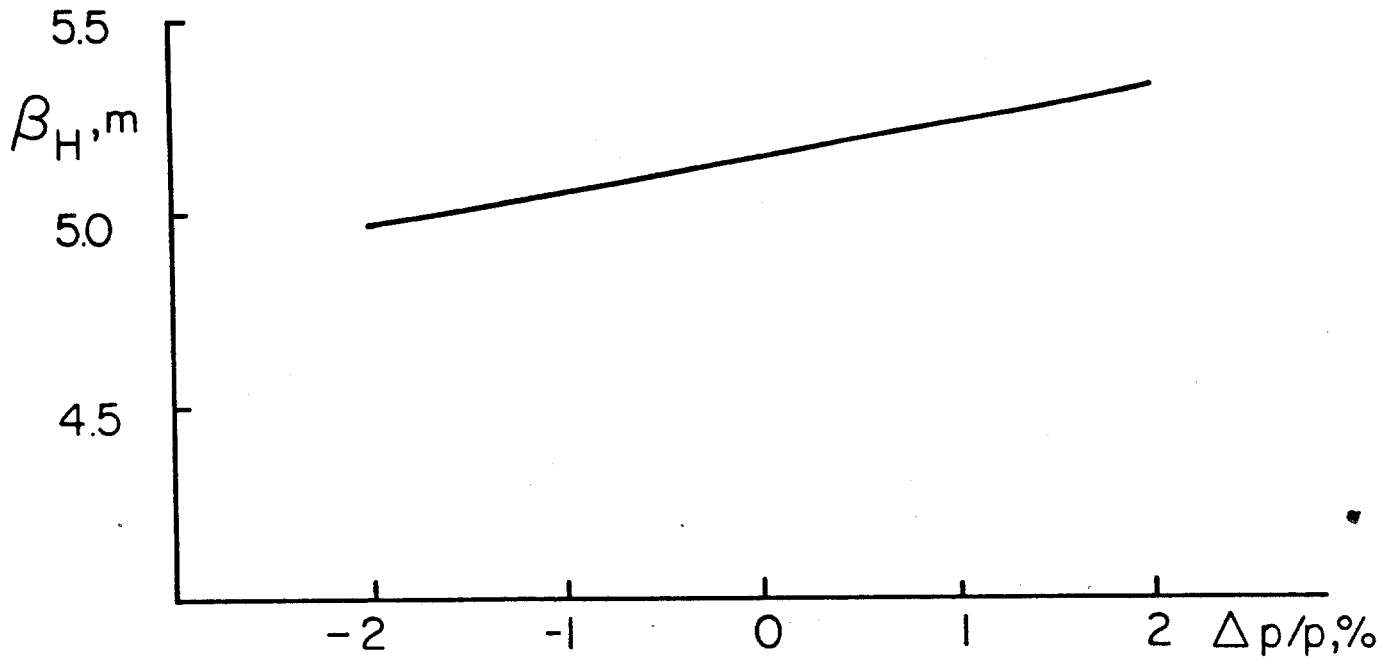
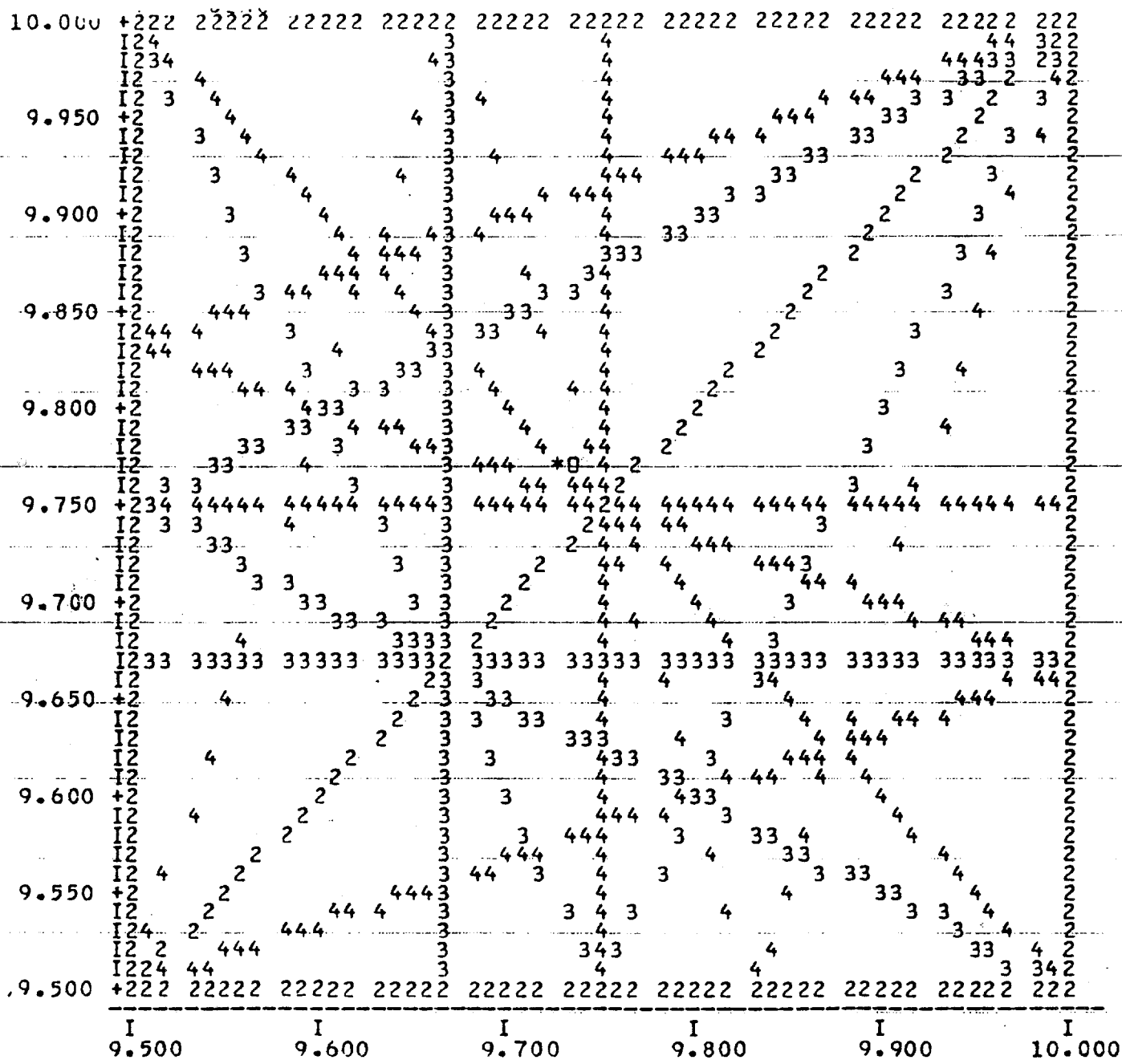


Figure 4-10



QX = 9.7300

QY = 9.7700

### Tune Diagram

Figure 4-11

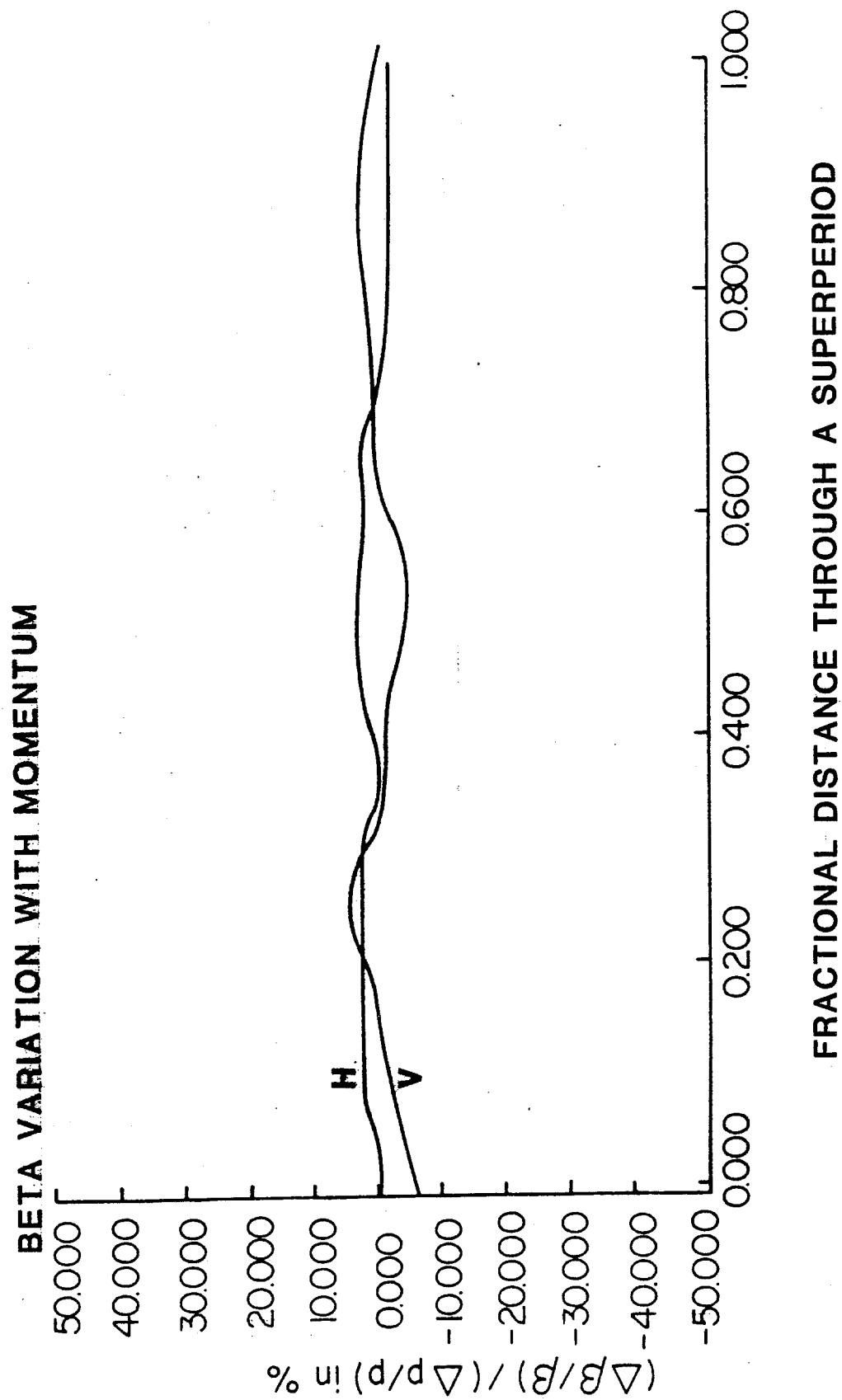


Figure 4-12

- ii) Only one current bus is required for all the dipoles. The current is 1175.6 A and a regulation of 0.01%. No shunts are needed, even for closed-orbit correction.
- iii) There is one bus for the regular horizontally focusing quads (QF) and one for the vertically focusing quads (QD). The two buses are individually controlled. The current is 240 for QF and 235 for QD. Power supply regulation is 0.01%. No shunts are required. Once the 60° phase advance/cell has been empirically obtained during the early days of operation, these quadrupole settings should remain unchanged.
- iv) The special quadrupoles QF1, QF2, QD1 and QD2 in the long straight sections are connected together to a common power supply bus with a maximum current of 290 A; each of them has a shunt to drive the current down 55 A. The regulation is, as usual, 0.01% in current.
- v) The special large-aperture quadrupoles QF3 and QD3 are connected to the dipole bus, which provides 1175.6 A, but on top of this individual power supplies for the range -50 to 100 A are added. The regulation requirement for this addition is 0.05%.
- vi) The small aperture quads QF3 and QD3 in the long straight sections are connected respectively to the QF and the QD buses, but each of them carries an individual shunt with a current range of -40 A and a regulation of 0.05%.

#### 4.9 Bunch Rotation and Other RF Manipulation

In order to evaluate the effectiveness of the debunching process and thus to determine the momentum spread of  $\bar{p}$ 's that can be accepted at production, extensive computer simulations of the rotation and debunching sequences have been carried out. The following features have been included:

- (i) The antiproton bunches, at the moment they have been generated at the target, have the same longitudinal distribution as the proton bunches, that is, an rms bunch length of 5 cm.
- (ii) The  $\bar{p}$ 's traverse a dispersionless drift of nearly 300 m between the target and the first rf cavity. The rf voltage is to be generated by eight cavities located immediately following the injection septum.
- (iii) Three values of  $\eta$  were used to test the dependence of the rotation effectiveness versus the magnitude of  $\eta$ . A value of -0.002 was used with an rf voltage of 2 MV and a value of -0.004 was used with an rf voltage of 4 MV. For these two

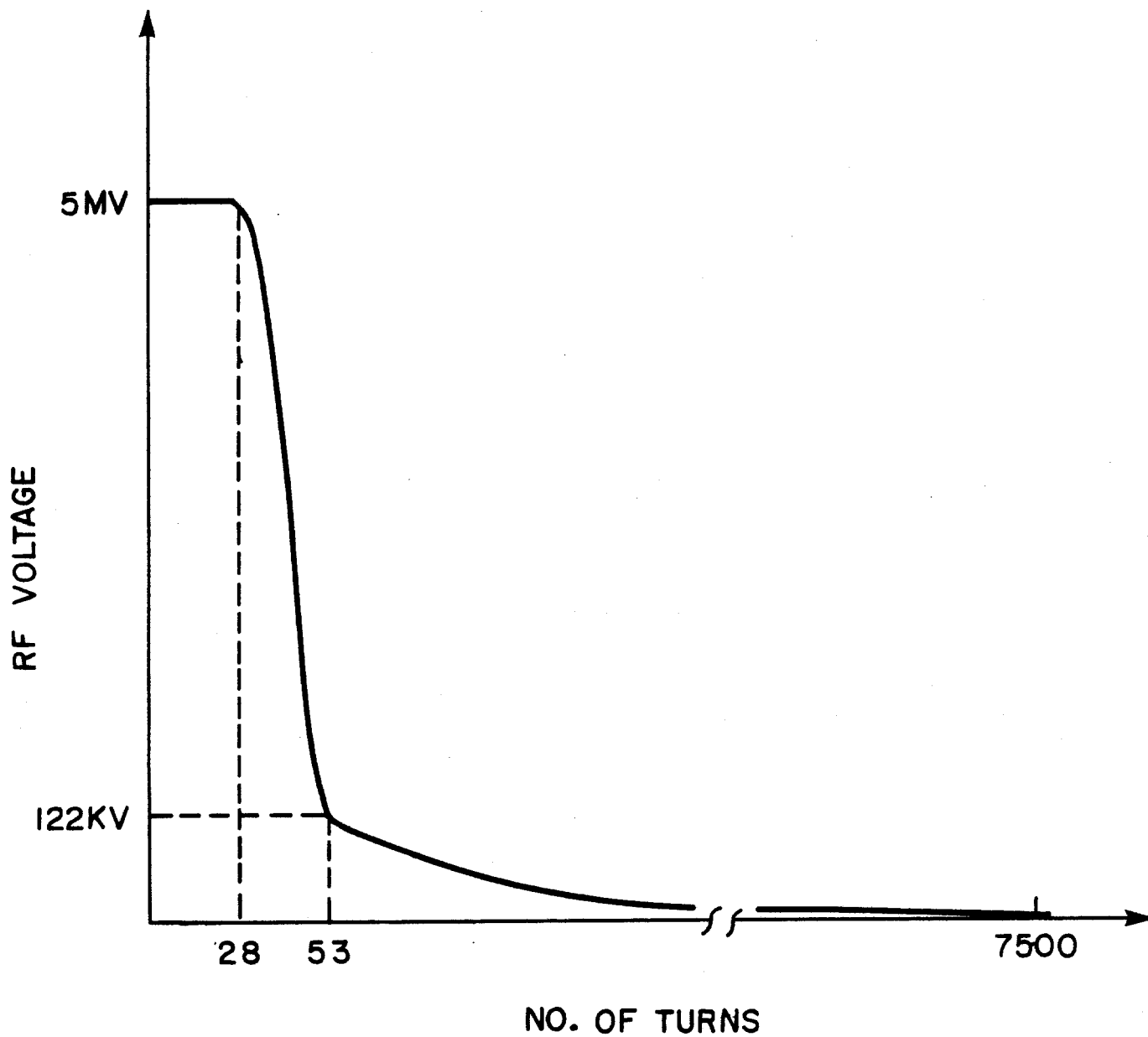
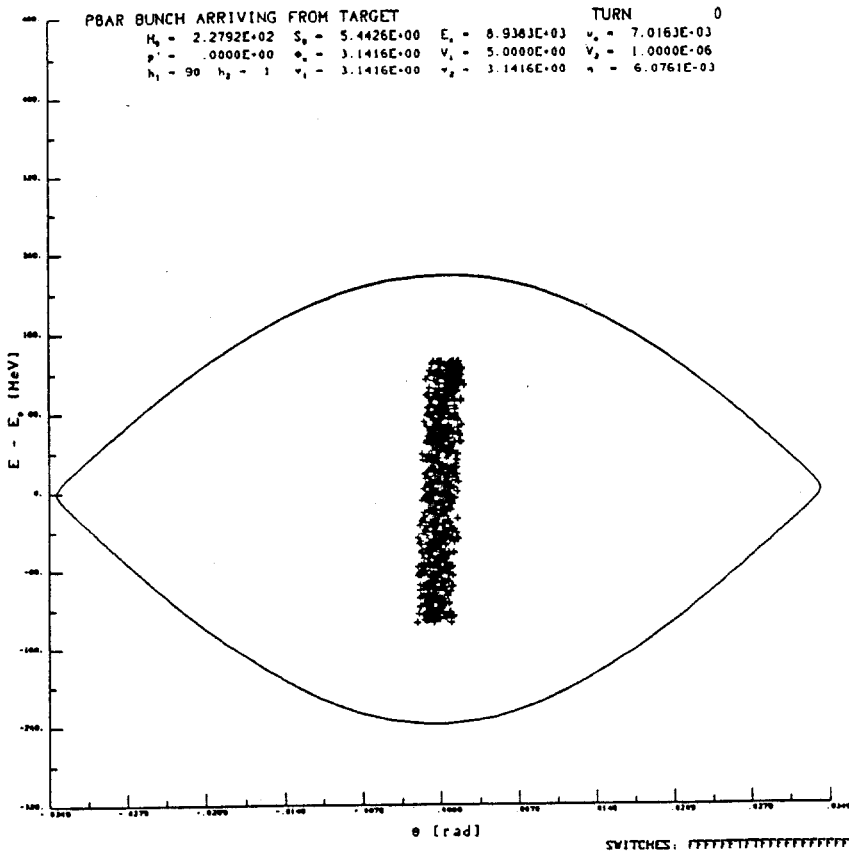
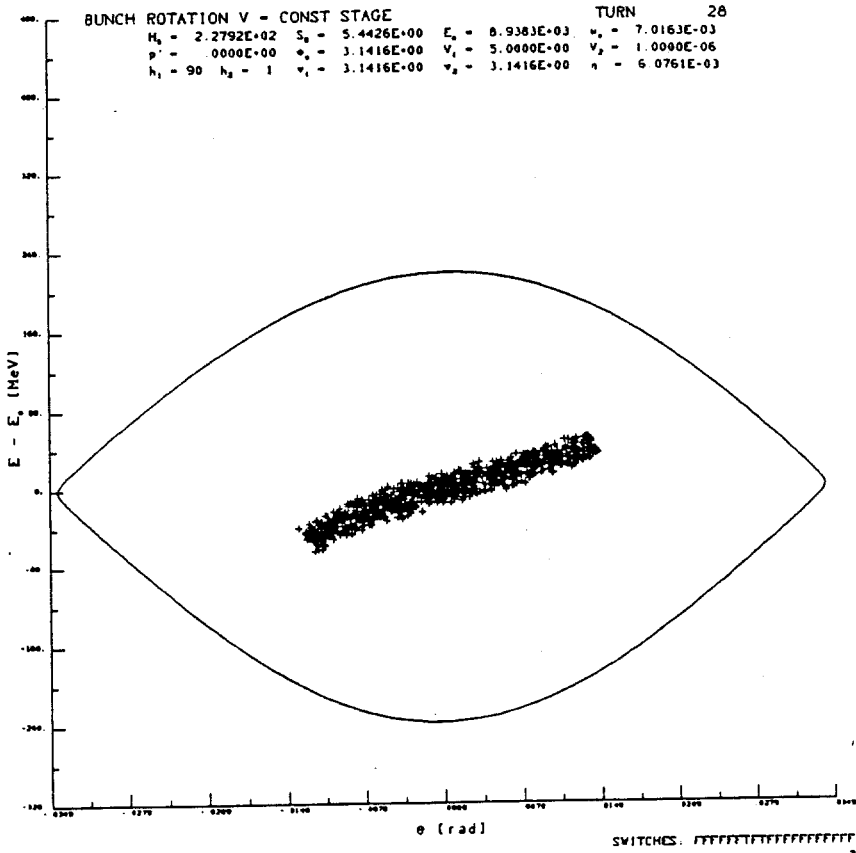


Figure 4-13 RF voltage program for the high gradient system in the Debuncher.



a) Antiproton bunch at injection into a Debuncher bucket produced by 5 mV



b) Bunch after 47.5  $\mu\text{sec}$ , at end of 5 mV portion of rf voltage program.

Figure 4-14 Phase-space during debunching.



cases an initial  $\Delta p/p=4\%$  was assumed. The simulation for the actual design case has  $\eta=0.006$  and an initial momentum spread of 3%; the maximum rf voltage was taken to be 5 MV. The results do not depend very much on the value of  $\eta$  although the case of  $\eta=-0.002$  is somewhat worse.

- (iv) The bunches are allowed to rotate for 20-35 turns while the voltage is kept constant. The rotation was about  $45-60^\circ$ .
- (v) The voltage is then dropped to approximately 100-120 kV in 30-35 turns (1 turn = 1.6  $\mu$ sec) to form a bucket matched in shape to the beam bunch, which has evolved into a distorted S-shape that extends over  $\pm 90^\circ$  in synchrotron phase.
- (vi) The voltage is slowly reduced to 5 kV and then abruptly turned off.

A debunching time of 12 msec was chosen, since longer times did not significantly reduce the momentum spread, while shorter times did increase the momentum spread. The final momentum spread is not sensitive to the other details of the time dependence of the rf voltage except during the early stage of rotation. The rf voltage program for the rotation and debunching operations is shown in Fig. 4-13 for the actual design case of  $\eta=-0.006$  and  $\Delta p/p=3\%$ . Figures 4-14 shows the beam shape at the end of some of the steps for  $\Delta p/p=3\%$ . If the debunching could be done without dilution, 95% of the beam would be contained within a momentum spread of 0.17%. Computer simulations show that the debunched momentum spread is 0.23%. The 30% factor of dilution has several causes. It is caused in part by nonlinearities of phase oscillations of particles captured within an rf bucket and in part by the variations of  $\gamma^{-2}$  of the particles and the momentum compaction factor  $\gamma_t^{-2}$  with energy. These variations and the presence of sextupole corrections in the ring lattice were taken into account in the simulations (see Fig. 4-9).

Calculations were done with other initial momentum spreads for the design case. The initial rf voltage of 5 MV and the final rf voltage of 5 kV were kept fixed for these calculations. These results are shown in Fig. 4-15. The numbers in brackets are a measure of the dilution. The choice of 5 MV seems to be optimal for  $\Delta p/p=3\%$ . The momentum spread of the  $\bar{p}$  beam will be limited to 3% by collimation prior to injection into the Debuncher. The Debuncher itself has a momentum aperture of over 4%. It may be possible to reduce the debunched beam momentum spread further if the rf voltage can be reduced adiabatically to a value much less than 5 kV.

Harmonics of twice and three times the fundamental frequency were added in the simulations. Significant improvement was found only for larger initial momentum spread.

A summary of the rf parameters is given in Table 4-VI.

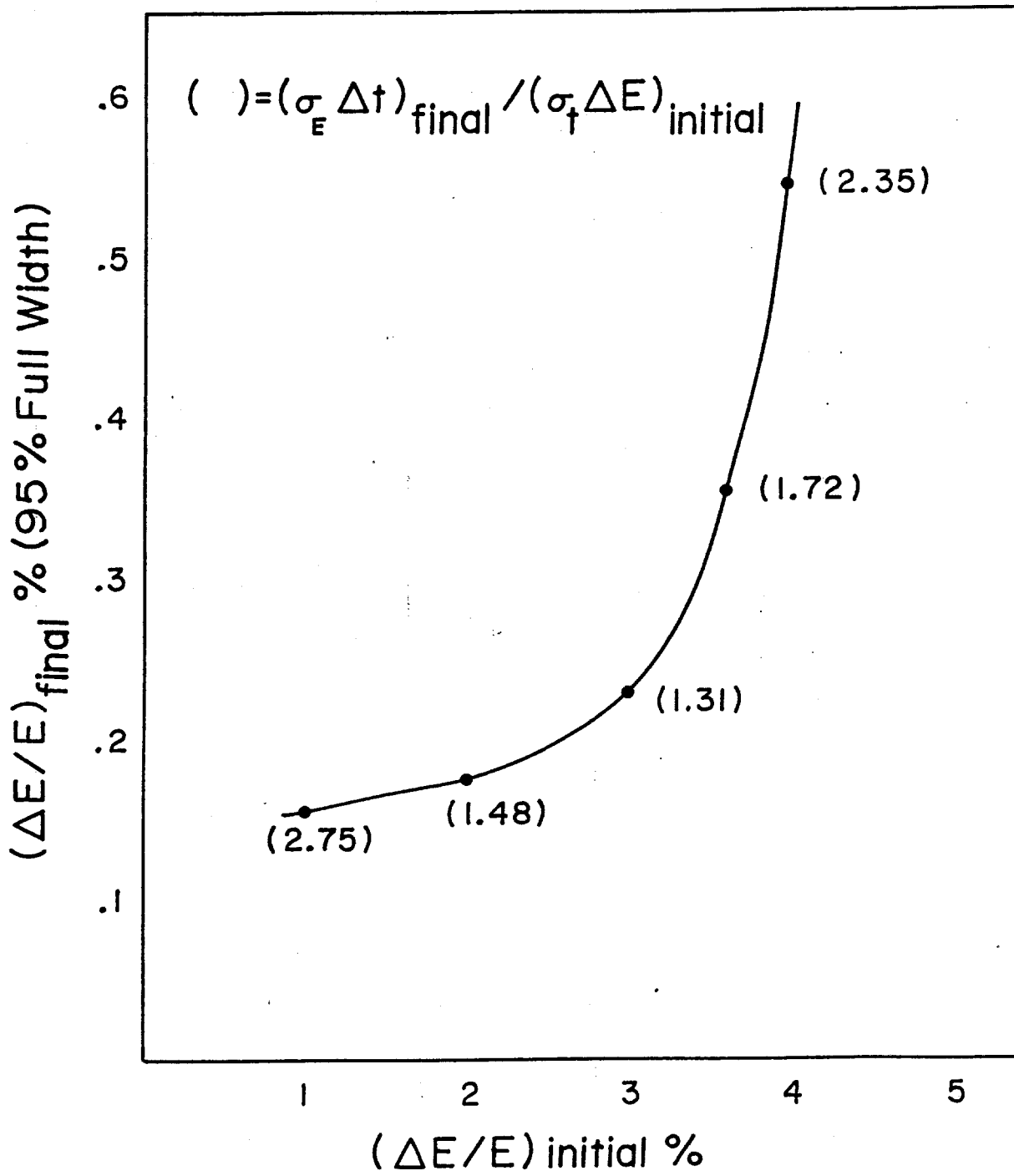


Figure 4-15

TABLE 4-VI DEBUNCHER RF PARAMETERS

|                                                     |                 |
|-----------------------------------------------------|-----------------|
| Kinetic Energy                                      | 8.0 GeV         |
| Number of antiproton bunches                        | 80              |
| Total number of antiprotons ( $\Delta p/p=3\%$ )    | $7 \times 10^7$ |
| Momentum aperture, $\Delta p/p$ (full width)        | 4%              |
| Bunch width (full)                                  | <1 nsec         |
| Transition $\gamma$ ( $\gamma_t$ )                  | 7.65            |
| Mixing factor, $\eta = \gamma_t^{-2} - \gamma^{-2}$ | .006            |
| RF frequency                                        | 53.1035 MHz     |
| RF harmonic number (h)                              | 90              |
| Revolution period                                   | 1.695 $\mu$ sec |
| Maximum voltage                                     | 5.0 MV          |
| RF voltage, end of rotation                         | 122.5 kV        |
| RF voltage, end of debunching                       | 5.0 kV          |
| Time required for rotation                          | .103 msec       |
| Time required for debunching                        | 12.712 msec     |

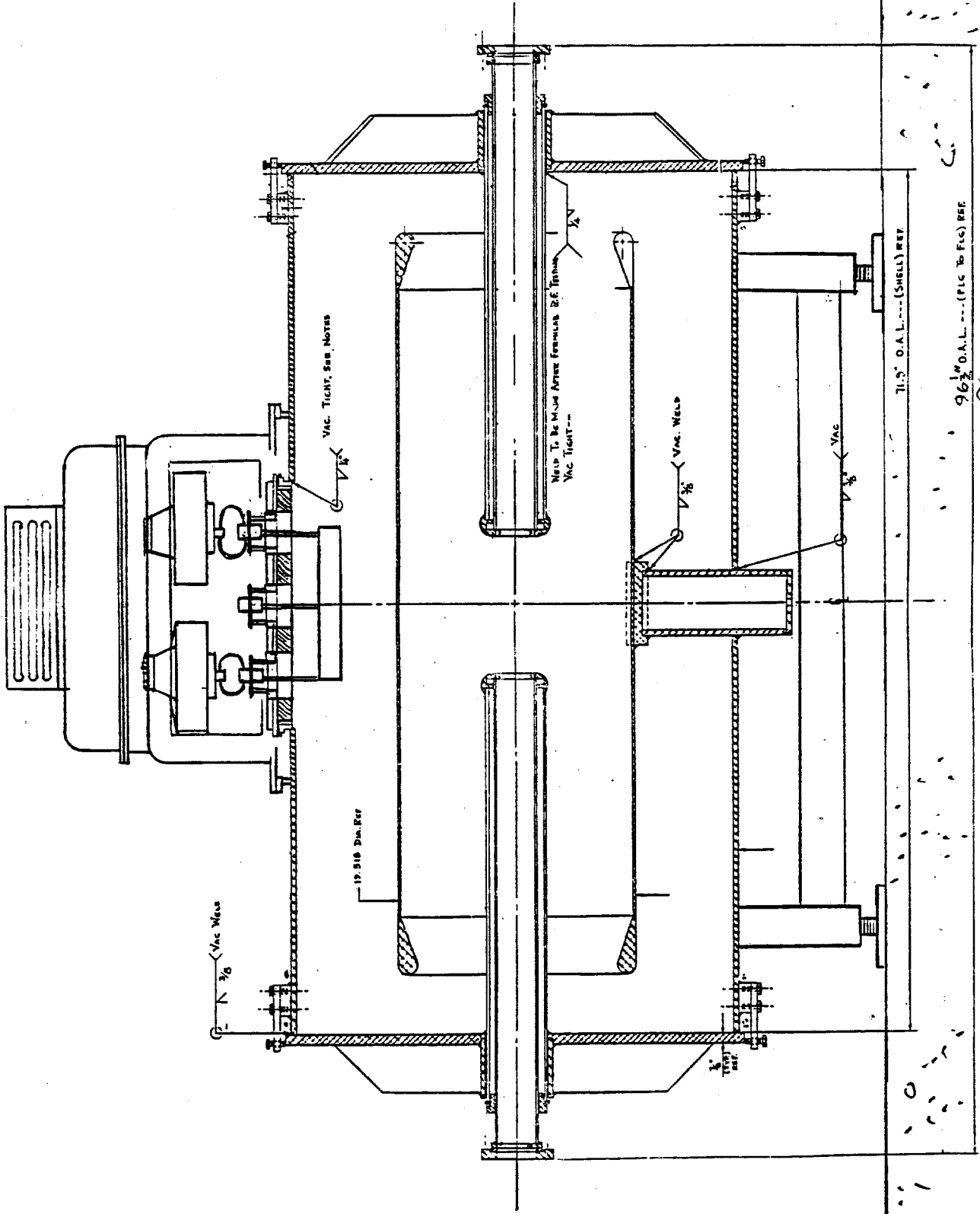
A broad-band, low-frequency rf system is operated to preserve a gap in the otherwise debunched beam. A 200 nsec gap is needed if the beam is to be transferred to the smaller Accumulator without loss. The rf system to make such a gap is described in Section 4.11.

#### 4.10 RF Systems for Bunch Rotation and Debunching

The design criteria for the antiproton Debuncher rf are:

- (i) Voltage gain per turn approximately 5 MV.
- (ii) Maximum pulse length 100  $\mu$ sec (duty factor  $5 \times 10^{-5}$ ).
- (iii) RF voltage pulse fall time from 5.0 MV to 120 kV, 50  $\mu$ sec.
- (iv) Pulse repetition rate 0.5 Hz.
- (v) Minimum voltage gain per turn  $\leq 5$  kV.
- (vi) Adiabatic reduction of voltage from 120 kV to  $\leq 5$  kV in a time of 5 to 20 msec under program control.

A representative rf voltage waveform was shown in Fig. 4-13. The design is simplified by the fact that the beam intensity will not exceed  $10^{10}$  particles when the rf voltage is on. Of the particles that emerge from the production target when it is struck by  $2 \times 10^{12}$  120-GeV protons, approximately  $2 \times 10^{10}$  are within the acceptance of the beam transport and the Debuncher. Some 90% of these particles are mesons, of which 50% decay before reaching the injection straight section. After each successive turn, 63% of the remaining mesons decay. The remainder of the particles that reach the center of the injection straight section consist of muons,



CROSS SECTION  
1/4" = 1"

Figure 4-16a

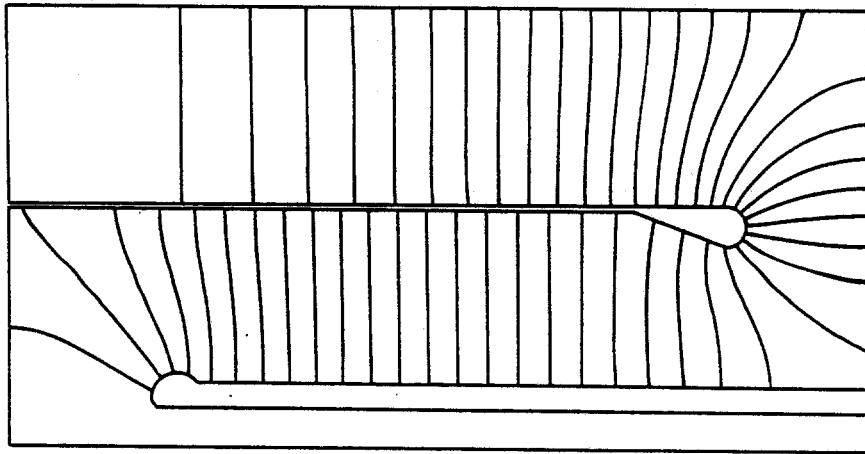


Figure 4-16b Electric field multiplied by radius as calculated by the program SUPERFISH

principally from pion decay, and electrons produced in showers in the target. The electrons lose 30 MeV per turn through synchrotron radiation and spiral out of the vacuum chamber within 20 turns.

The large rf voltage, low beam loading and small duty factor favor an accelerating cavity with a very high Q, hence a high shunt impedance, which requires very little rf drive power. But the short fall time of the rf voltage pulse is not obtained easily with a high-Q structure. Moreover, the physical size of high Q structures operating in the 53-MHz region would require much larger enclosures than are under consideration.

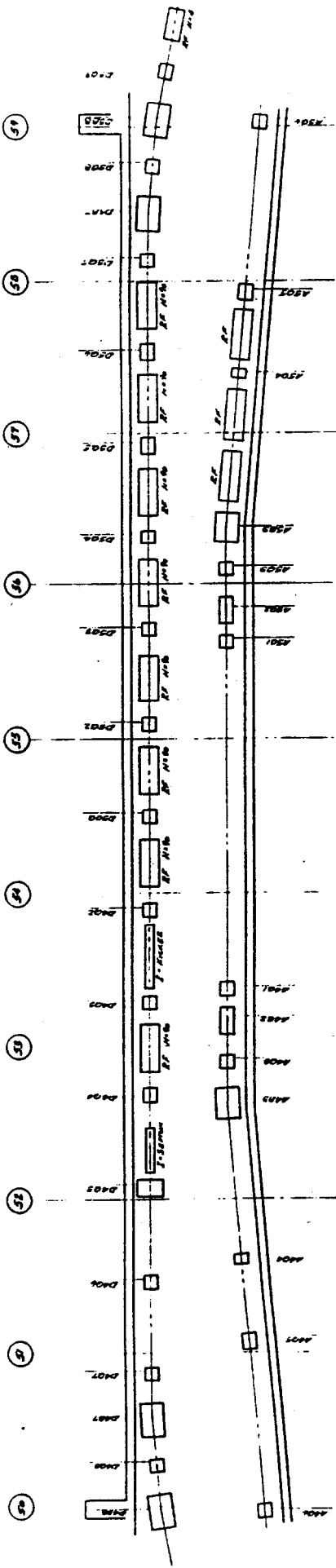
A compromise structure, which contains an intermediate cylinder that reduces both the Q and the physical size, is shown in Fig. 4-16a. Fig. 4-16b shows a SUPERFISH plot of the electric fields within one-quarter of the structure. The entire volume of each cavity will be evacuated, with rf power coupled through two small ceramic windows at the top. The plate through which rf power is introduced serves as a bedplate for the high-power driver amplifiers, which are mounted directly on top of the cavity and are completely enclosed. Thus high-power rf transmission lines are not needed and rf leakage is less likely. This may be important because rf noise could adversely affect stochastic cooling. Each cavity is driven by two relatively small 10-kW triodes operating in a cathode-driven grounded-grid configuration. In this configuration, the tubes are capable of delivering very large peak rf currents during the short pulse. Because the pulse is short and the duty factor is low, the average anode dissipation is only a few hundred watts.

The rf voltage is reduced quickly by reversing the phase of the power-amplifier excitation and raising the excitation amplitude to a very high level. The high peak-power capability of the tubes is used to "drive" the cavities off, even though the cavity time-constant is longer than the required turn-off time of 50  $\mu$ sec.

The peak rf voltage that each cavity can develop has been calculated to be larger than 650 kV. Eight of these 1.8 m long cavities provide the required 5 MV. They are located in the long straight section immediately following injection from the target. The location of these cavities is shown in Fig. 4-17.

In order to reduce the rf voltage down to 5 kV or less during the adiabatic-debunching part of the rf program, six of the cavities are turned off and two of the cavities are held at 100 kV and their relative phases each changed by 90° in opposite directions. The resultant rf voltage gradually reaches a small value. This is done to avoid instabilities at low rf voltage that might arise from multipactoring.

In order to provide the structural rigidity necessary for complete evacuation and to reduce material costs, the cavities will be constructed from aluminum.



PLAN — BUILDING 50

### Injection Straight Section Of The Debuncher

Figure 4-17

#### 4.11 Gap-Preserving RF

Because the Debuncher circumference is larger than that of the Accumulator, antiprotons will be lost in the transfer to the Accumulator unless there is a gap in the Debuncher beam. Given the difference in circumference between the two rings and the need to allow for the fall time of the injection kicker, a gap greater than 200 nsec is needed.

An adequate gap can be created in the beam by a "barrier bucket" that excludes particles from its interior. It is created by a voltage that traces out a single complete sinusoidal oscillation for one-quarter of the rotation period and then becomes zero for the remaining three-quarters of the period. A sketch of this waveform is shown in Fig. 4-18. The voltage waveform repeats itself every turn. The phase of the voltage is chosen so that it establishes an unstable fixed point between two back-to-back half-bucket separatrices. If the bucket height exceeds the beam energy spread, the beam will be forced away from the unstable fixed point by a distance determined by the ratio of the bucket height to the energy spread. The rf voltage is chosen so that the beam is excluded from a region between  $\pm\pi/2$  radians in the "barrier bucket". This will create a gap of 221 nsec, as shown in Fig. 4-18. The peak amplitude required is 890 V. The Fourier series expansion of such a voltage waveform is given by

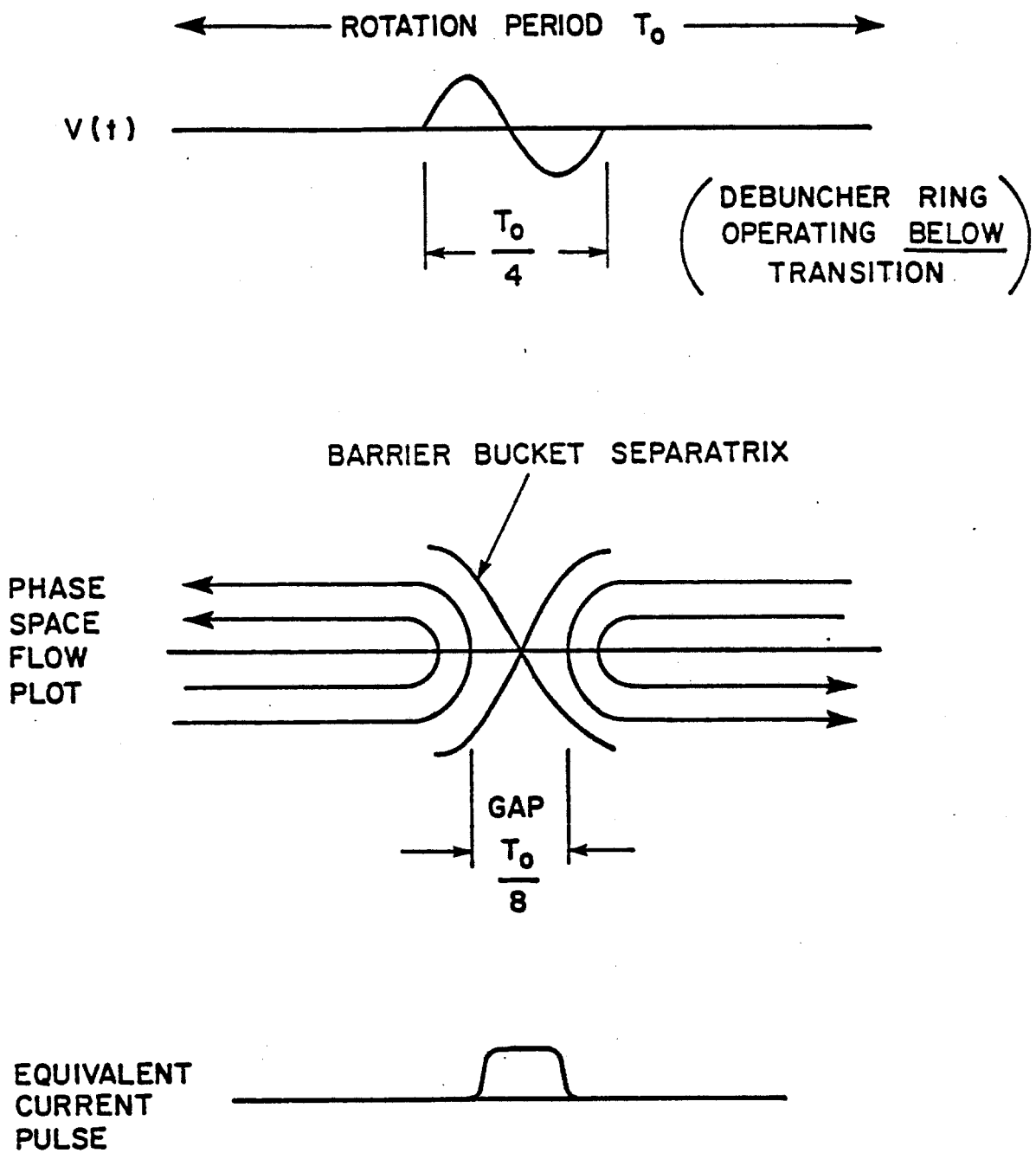
$$V(t) = 890 \frac{2h}{\pi} \sum_{n=1}^{\infty} \frac{\sin \pi n/h}{h^2 - n^2} \sin(n\omega_0 t),$$

where  $\omega_0 = 2\pi f = 3.59 \times 10^6$  rad/sec and  $h=4$ . At frequencies above the 31<sup>st</sup> harmonic (17.7 MHz) the required amplitudes are reduced by more than three orders of magnitude. Amplifiers with a bandwidth between 0.1 and 30 MHz which are capable of delivering 300 W in a 50-ohm load are readily available. The required rf system can be broken into 450-V units, each consisting of a ceramic gap loaded with a 50-ohm resistor and surrounded by a shielding enclosure containing about ten large MnZn ferrite rings. The average power delivered to this system is very small. Since the physical size of each unit is dictated by the volume of ferrite required, each unit is 0.5 m in length. Their location is shown in Fig. 4-17.

An additional bonus associated with installation of the "barrier bucket" rf system is that it can be used in the "normal"  $h=4$  mode to accelerate or decelerate 8-GeV protons across the ring aperture in tune-up testing of closed orbits and stochastic-cooling systems.

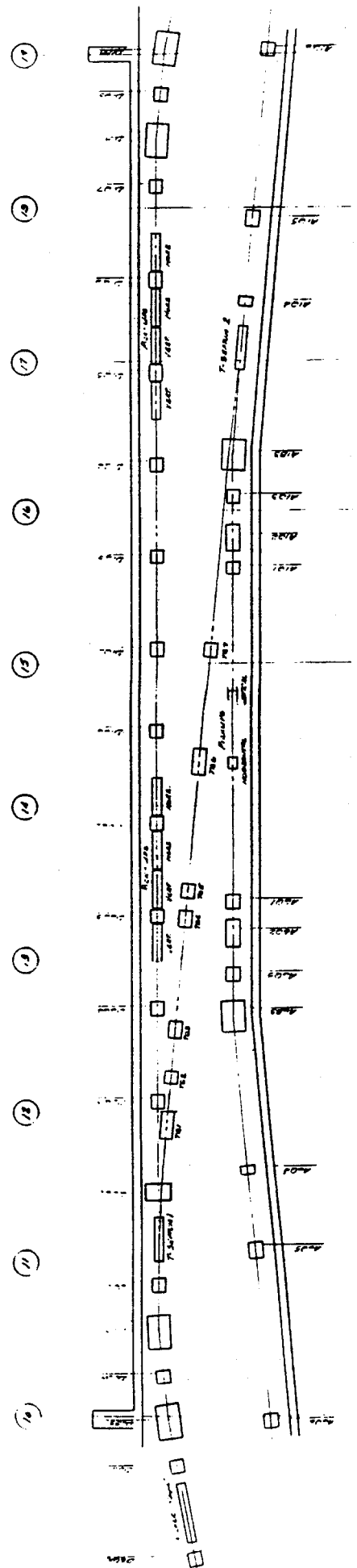
#### 4.12 Beam Injection and Extraction

4.12.1 Injection from the Target Station. The beam enters the Debuncher in the vertical plane at an angle of 50 mrad to the closed orbit. The injection path is exactly aligned with the central closed orbit of the



**Gap Preserving RF**

Figure 4-18



Plan - Drawing #10

### Beam Transfer From Debuncher To Accumulator

Figure 4-19

Debuncher. The beam first enters QF3, which has a large aperture to accommodate both the injected and the circulating beam. The circulating beam goes through the center of the quad, but the injected beam enters the quad with a vertical displacement of 5 in. at the upstream end and an angle of 50 mrad. A septum magnet located after QF3 brings the beam down to a vertical separation of 2 in. and parallel to the ring orbit. A kicker magnet between QF2 and QD1 brings finally the beam onto the reference orbit. The kicker and septum magnets parameters are given in Table 4-VII and are shown in Fig. 4-17. The injection channel has been designed to accommodate a beam with momentum spread of 4% and transverse emittances of  $20\pi$  mm-mrad.

4.12.2 Debuncher to Accumulator Transfer. The beam transfer between the Debuncher and the Accumulator is a horizontal transfer taking place in the 10 straight section. Extraction from the Debuncher is accomplished with a kicker and a septum magnet, as shown in Fig. 4-19. The quadrupole after the septum magnet, QD3, has a large aperture to accommodate both the circulating and the extracted beam. This quad kicks the beam further to the inside of the ring toward the Accumulator. The horizontal displacement of the extracted beam from the magnet axis is 5 in. After extraction, the beam is transported to the Accumulator with no further bending through a string of 6 quadrupoles. At the Accumulator, the beam is injected onto a path displaced from the central momentum by  $\Delta p = +0.93\%$  with an 12-kG 7-ft long pulsed septum placed between A1B3 and A1S3. Finally the beam is kicked onto the proper orbit in the Accumulator with a 500-G, 7-ft long shutter kicker placed in the A20 straight section. The elements are discussed in more detail in Sec. 11.3. A plot of the lattice functions of the transfer line is shown in Fig. 11-5 and the list of elements is given in Table 11-IV.

4.12.3 Injection from the Booster. Injection into the Debuncher from the Booster is exactly the same as injection from the Target Hall. The beam is transported to the upstream end of the 30 straight section and injected downward into the Debuncher at an angle of 50 mrad, again passing through a large-aperture quadrupole D2Q5 and then into a septum magnet. Finally a kicker located between D2Q3 and D2Q2 puts the beam onto the reference orbit.

## 4.13 Betatron Cooling

4.13.1 Design Goal. The goal of the stochastic cooling in the Debuncher is to cool the beam emittance from  $20\pi$  mm-mrad to  $7\pi$  mm-mrad in both the horizontal and vertical planes. An emittance of  $7\pi$  mm-mrad is the assumed beam size that can be reliably transferred into the  $10\pi$  mm-mrad acceptance Accumulator ring with negligible beam loss. In addition to cooling the beam to fit into the Accumulator, it is desirable to make the beam injected into the Accumulator as small as possible. In the Accumulator the momentum stacking is done in part by a pickup that senses a particle's momentum by observing its position in a region of high dispersion. Betatron oscillations add undesired noise to this process.

4.13.2 Design Considerations. The betatron-cooling system is conceptually simple. It consists of a pickup that senses the positions in a zero-dispersion region and therefore measures only the betatron amplitudes of the particles. The signal is amplified and applied to a kicker an odd multiple of  $90^\circ$  away in betatron phase. At the kicker, the position displacement that was sensed has been converted into an angular displacement. This angular displacement is decreased by a correcting kick, which thus decreases the betatron amplitude. As is well known, the cooling of a single particle is hampered by the presence of the other particles, that create a noise signal (Schottky noise) that heats the particle. For a properly designed system, the net effect over many turns is that cooling is achieved.

The process of betatron cooling is conventionally described by the equation

$$\frac{d\varepsilon}{dt} = -\frac{W}{N}(2g-g^2(M+U))\varepsilon, \quad (4.1)$$

where  $\varepsilon$  is the betatron amplitude,  $W$  the amplifier bandwidth,  $N$  the number of particles,  $g$  the system gain,  $M$  the mixing factor and  $U$  the ratio of noise to signal power. The mixing factor  $M$  is given by

$$M = \frac{f^2 \psi(f) \Lambda}{2WN}, \quad (4.2)$$

where  $\psi(f)$  is the density of particles (number per Hz),  $f$  is the revolution frequency, and  $\Lambda$  is a constant of order unity ( $\Lambda = \ln 2$  if the gain is independent of frequency).

Stochastic cooling during the 2-sec Debuncher cycle is difficult because the mixing factor  $M$  is large compared to 1.  $M$  is inversely proportional to the dispersion  $\eta$ , where

$$\frac{\Delta f}{f} = \eta \frac{\Delta p}{p}, \quad (4.3)$$

The choice of the value of  $\eta$  was a compromise between the rf requirement for the bunch rotation (which favors a small  $\eta$ ) and stochastic cooling (which favors a large  $\eta$ ). The choice of  $\eta = +0.006$  leads to a mixing factor  $M$  of about 10 for the particles near the central momentum of the Debuncher, assuming a parabolic momentum distribution with a full width of  $\Delta p/p = 0.3\%$ .

Another problem is that the noise-to-signal ratio  $U$  tends to be large. The techniques to make  $U$  small are: 1) increase the beam signal as much as possible by using a large number of high-impedance pickups and 2) decrease the noise temperature by cooling the pickup terminating resistors and the preamplifiers.

The criterion for the thermal noise to be negligible is  $U \ll M$ . With the parameters of Table 4-VII below,

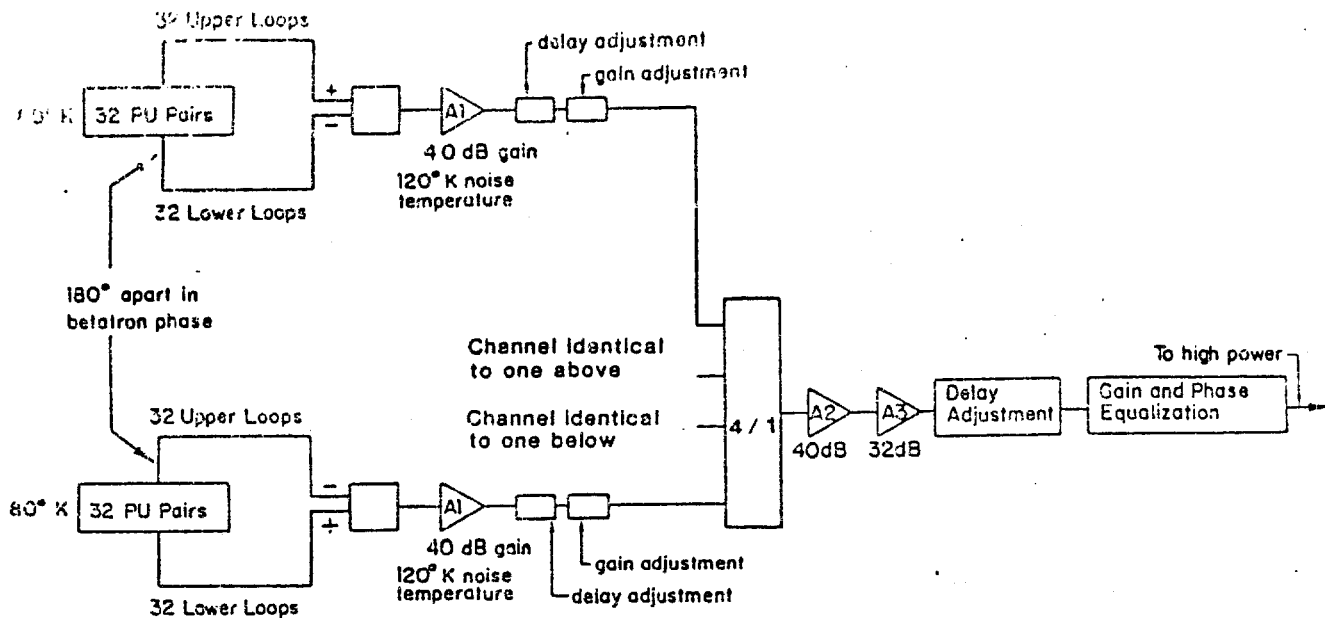
$$U = \frac{2K (\theta_R + \theta_A) h^2}{d^2 Z_0 e^2 f_0 n_p N \beta_p \bar{\epsilon}} \quad (4.4)$$

$$= 1.8 \text{ (initially) } ,$$

where  $K = 1.38 \times 10^{-23}$  Joules/°K,  $f_0 = 1/T =$  revolution frequency,  $\bar{\epsilon} =$  average beam size =  $8\pi$  mm-mrad initially. But, as the beam is cooled to  $\bar{\epsilon} = 0.8\pi$  mm-mrad,  $U$  will grow to 18, twice the value of  $M$ , the mixing factor. Thus cooling will initially proceed not limited by thermal noise, but as the beam cools, the effect of the Schottky and thermal noise become comparable (note that the cooling equation (4.1) is written in a deceptive form because it does not explicitly show the dependence of  $U$  on  $\bar{\epsilon}$ ).

A practical problem that occurs in fast stochastic cooling is that the power requirements are often very high. In the Debuncher, the best cooling rate is obtained for a power level of 1800W. But, as can be seen from Eq. (4.1), the gain can be decreased by a factor of 2 and the cooling rate will be only  $2g - g^2 = 3/4$  of the optimum rate. In the absence of suppression, the power will decrease by a factor of 4. In the case that signal suppression is important, the decrease in power can be even greater, because the system gain  $g$  increases more slowly than linearly with the amplifier gain. In a system with bad mixing like the Debuncher, most of the thermal power is between Schottky bands and is largely unaffected by signal suppression. In this case, the thermal power is therefore more nearly proportional to amplifier gain squared than to system gain squared ( $g^2$ ).

**4.13.3 Hardware.** For each of the two betatron-cooling systems, 4 sets of 32 pickup pairs are installed in straight section D10, and a similar set of kickers are installed in straight section D30. Both straight sections have zero dispersion. The pickup arrays are spaced out between the quadrupoles in a manner such that 2 sets are roughly  $180^\circ$  out of phase with the other two. These signals are therefore combined with inverted phase. The signal is then amplified and sent to the kicker region which is  $3 \frac{1}{4}$  betatron oscillations away. The pickup termination resistors are cooled to  $77^\circ\text{K}$ , as are the preamplifiers. A block diagram of the betatron cooling system is shown in Fig. 4-20. In brief, the pickup signal from 32 upper plate pickups is combined with 32 lower plate signals to provide a difference



Debuncher Betatron Cooling Systems

2-4 GHz Horizontal and Vertical Systems are Identical.

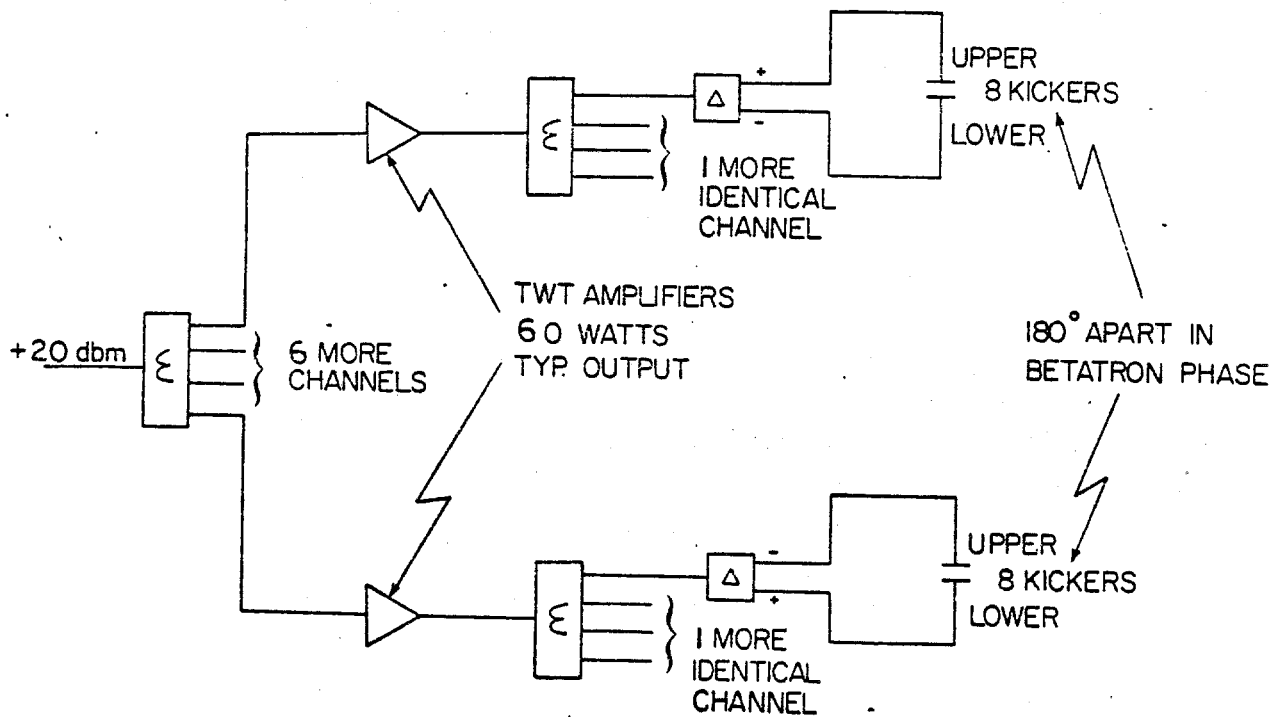


Figure 4-20

signal proportional to the position displacement of the beam. The signals from each set of 32 pickups amplified 40 dB are combined in an 4-fold combiner. Each combiner input has an adjustment for amplitude and delay. After combination the signal is further amplified by 72 dB to a level of about 25 dBm. An overall delay adjustment is followed by a gain and phase compensating circuit, to partially cancel the variations in the TWT (traveling wave tube) gain characteristics. The power is then split to drive two sets of TWT's, each of which drives an array of 16 kickers.

Table 4-VII lists some of the parameters of the betatron cooling systems. The characteristics of the hardware components are similar to those in the Accumulator, these characteristics are discussed in more detail in Section 5.4. The overall layout of the stochastic cooling system in one straight section was shown in Fig. 4-7.

4.13.4 Computer Simulation<sup>5</sup>. A simulation of the betatron cooling in the Debuncher was made to calculate the expected system performance. Included in the simulation were the pickup and kicker response functions, transit-time differences of the electrical signal and particles between pickup and kicker, and signal suppression. The amplifier was modeled as a physically unrealizable ideal amplifier having a gain  $g_A$  from 2 to 4 GHz and zero elsewhere. It was assumed that  $g_A$  was purely real. While the amplifier model was not realistic, measurements of the TWT tube amplifiers in the 1-2 GHz range show that, when externally phase compensated, these tubes can provide gain and phase characteristics that lead to cooling rates equal to or better than the 1-2 GHz "ideal" amplifier model used above. The initial  $\bar{p}$  distribution was taken from Fig. 3-4. It was assumed that the Debuncher had an acceptance of  $25\pi$  mm-mrad but that the transport line had already limited the beam size to  $20\pi$  mm-mrad. The total output power was limited to 500W. The gain was continually adjusted to provide the best cooling within the 500W limit.

Figure 4-21 shows the initial and final beam distributions for particles at the central momentum. Ninety-nine per cent of the particles fall within an emittance of  $7\pi$  mm-mrad. Also shown is the final curve for particles with a momentum offset of 0.075%, or halfway to the edge of the distribution. The cooling of these particles is somewhat better since they have a somewhat lower density, i.e., less Schottky noise. Since the noise figure assumed is somewhat speculative, Fig. 4-22 compares the final spectrum for design case  $\theta_A + \theta_R = 200^\circ\text{K}$ . If the noise figures were worse because of the pickup sensitivity being less than supposed, the kickers would presumably be less sensitive in the same ratio. In this case, the total dissipated power would be larger than the design case of 500W. Figure 4-23 is a comparison of the final distribution for different power levels assuming the design case noise figure ( $\theta_A + \theta_R = 200^\circ\text{K}$ ). As previously stated, there is little advantage in running at power levels corresponding to the optimum gain.

As designed, the stochastic cooling system for the Debuncher will cool the beam emittance by about an order of magnitude. If the system fails to

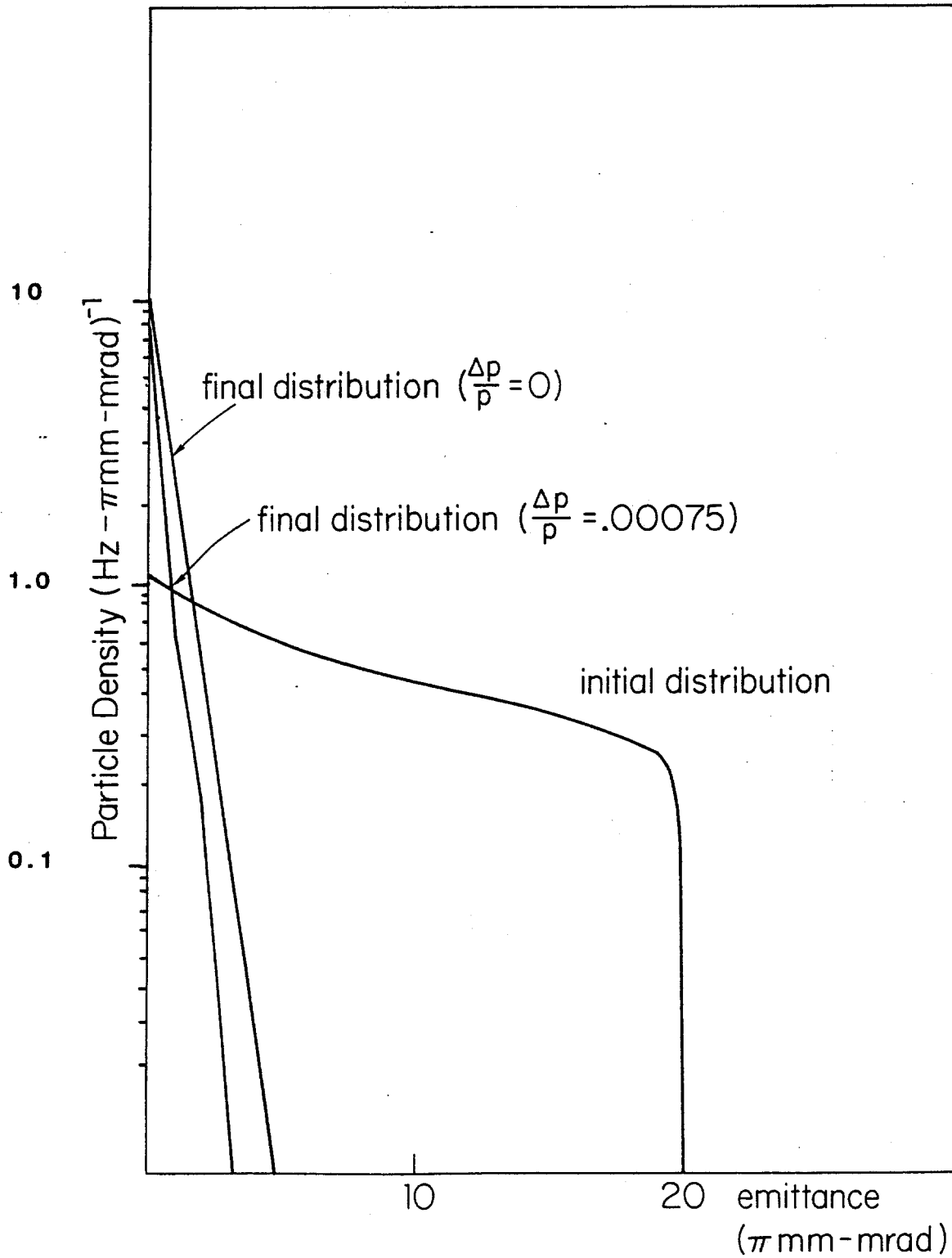


Figure 4-21

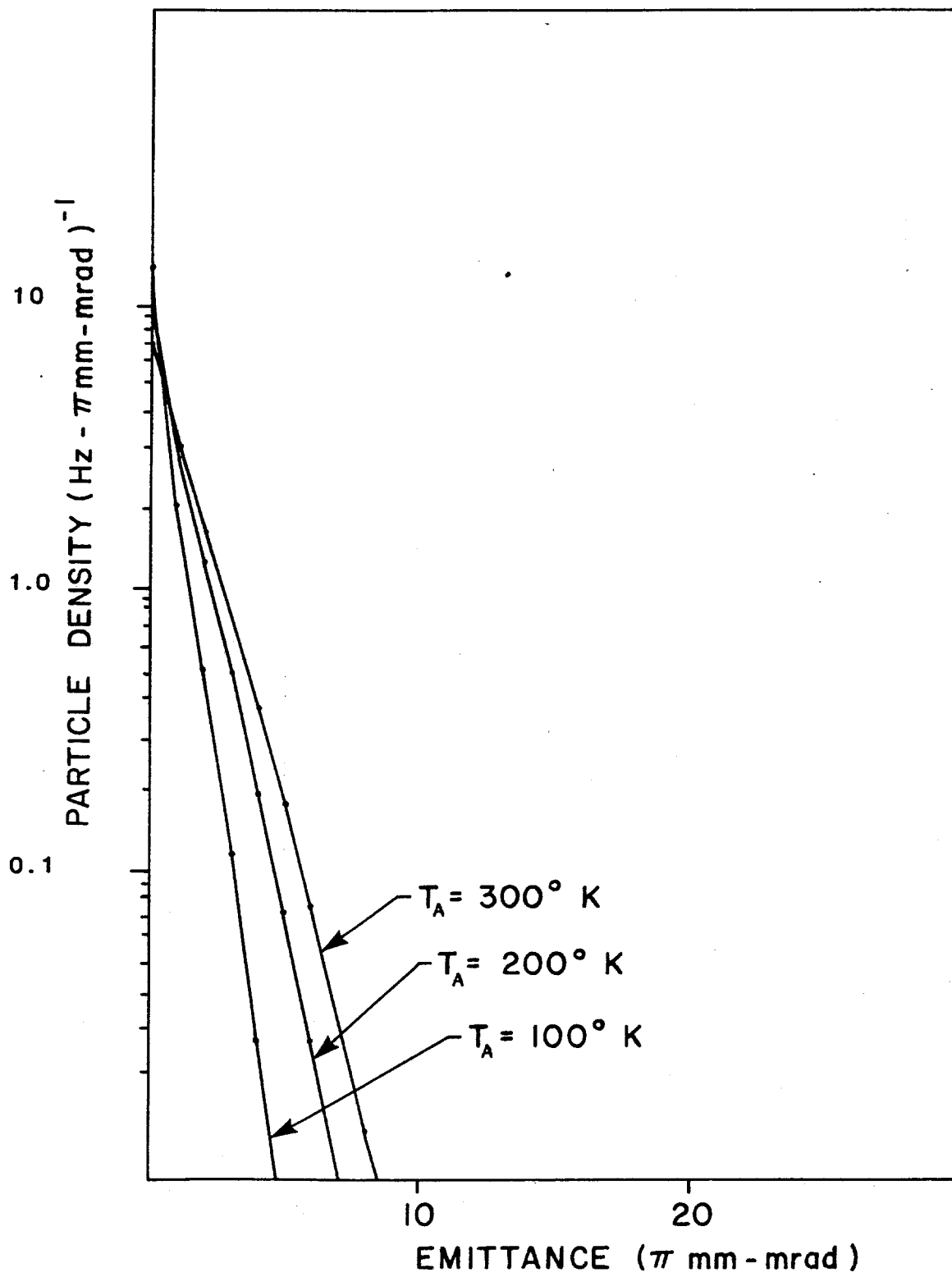


Figure 4-22

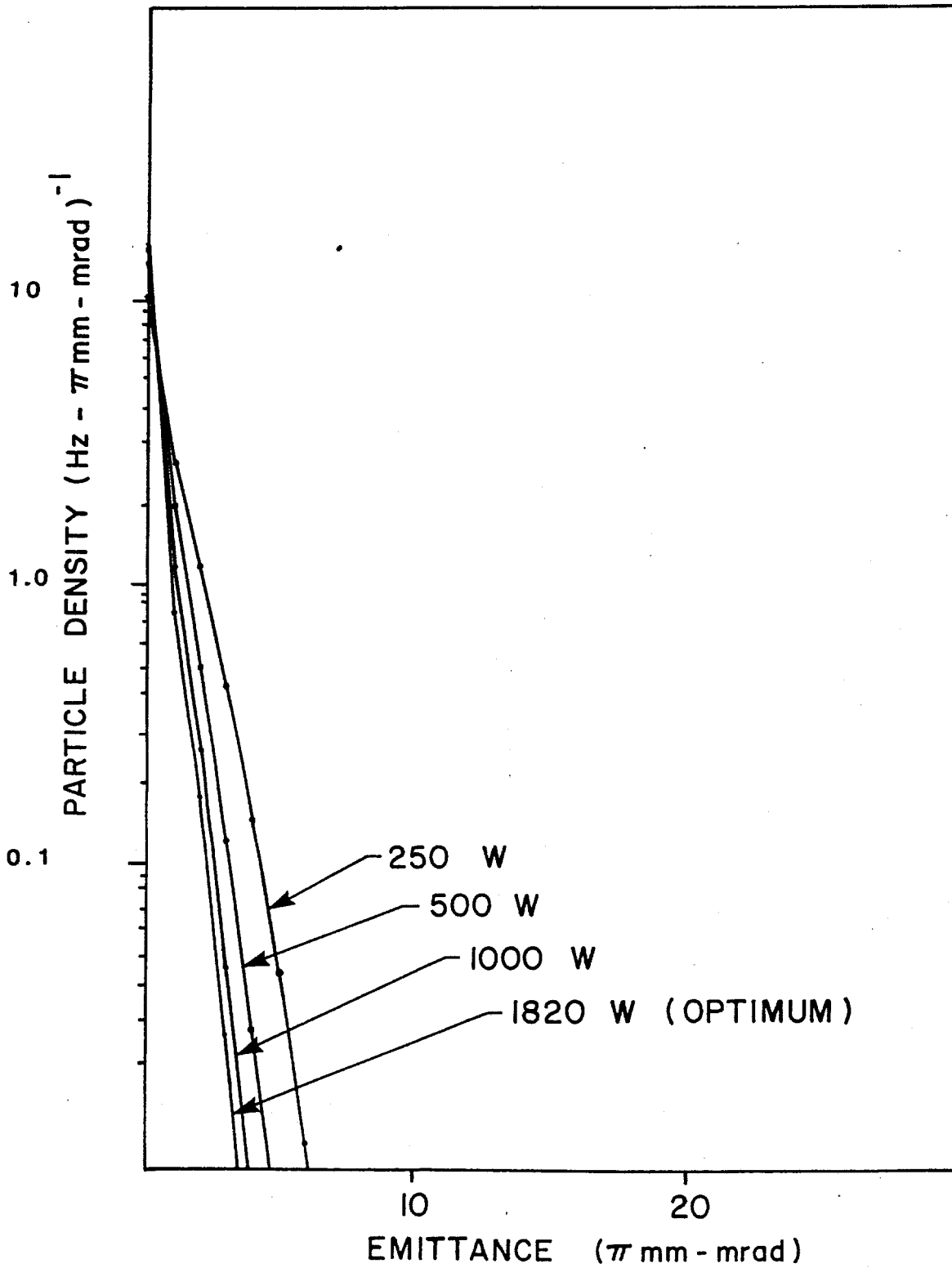


Figure 4-23

perform as designed, there is a substantial margin of safety in getting the beam to  $7\pi$  mm-mrad for transfer into the accumulator.

TABLE 4-VII BETATRON-COOLING SYSTEM PARAMETERS (EACH SYSTEM)

|                                                       |                   |
|-------------------------------------------------------|-------------------|
| Frequency band                                        | 2-4 GHz           |
| Number of pickup pairs (loops)                        | 128               |
| Pickup Characteristic Impedance (odd mode)            | $83\Omega$        |
| Pickup Sensitivity $d(0,0)$                           | 1.59              |
| Pickup resistor noise temperature ( $\theta_R$ )      | 80K               |
| Amplifier equivalent noise temperature ( $\theta_A$ ) | 40K               |
| Amplifier gain (net) (variable)                       | 138 dB (variable) |
| Output Power                                          |                   |
| -Schottky                                             | 100 W (typical)   |
| -Thermal                                              | 400 W (typical)   |
| -Total                                                | 500 W             |
| Number of TWT's                                       | 8                 |
| Number of kicker pairs (loops)                        | 128               |
| Kicker characteristic impedance                       | $83\Omega$        |
| Kicker sensitivity $d(0,0)$                           | 1.59              |
| Spare time delay with foam heliix ( $\beta=0.89$ )    | 45 ns             |